CLIMATE CHANGE SCENARIOS AND SEA LEVEL RISE ESTIMATES FOR THE CALIFORNIA 2009 CLIMATE CHANGE SCENARIOS ASSESSMENT

A Paper From:
California Climate Change Center

Prepared By:
Dan Cayan[1,2], Mary Tyree[1], Mike Dettinger[2,1], Hugo Hidalgo[1], Tapash Das[1], Ed Maurer[3], Peter Bromirski[1], Nicholas Graham[5,1], and Reinhard Flick[4,1]

[1] Scripps Institution of Oceanography, University of California San Diego
[2] U. S. Geological Survey
[3] Santa Clara University
[4] California Department of Boating and Waterways
[5] Hydrologic Research Center

FINAL PAPER

DISCLAIMER

This paper was prepared as the result of work sponsored by the California Energy Commission (Energy Commission), California Ocean Protection Council (OPC), and the California Environmental Protection Agency (Cal/EPA). It does not necessarily represent the views of the Energy Commission, OPC, Cal/EPA, their employees, or the State of California. The Energy Commission, OPC, Cal/EPA, the State of California, their employees, contractors, and subcontractors make no warrant, express or implied, and assume no legal liability for the information in this paper; nor does any party represent that the uses of this information will not infringe upon privately owned rights. This paper has not been approved or disapproved by the California Energy Commission, OPC, or Cal/EPA, nor has the California Energy Commission, OPC, or Cal/EPA passed upon the accuracy or adequacy of the information in this paper.

Arnold Schwarzenegger, *Governor*

August 2009
CEC-500-2009-014-F

Acknowledgments

Support for Dan Cayan, Hugo Hidalgo, Mary Tyree, and Ed Maurer was provided by the State of California through the California Energy Commission's Public Interest Energy Research (PIER) Program. Dan Cayan and Mary Tyree were also supported by the National Oceanic and Atmospheric Administration's Regional Integrated Sciences and Assessments (RISA) Program through the California Applications Center, the California Department of Boating and Waterways, and the California Ocean Protection Council. Tapash Das and Mary Tyree were supported by the Lawrence Livermore National Laboratory. Mike Dettinger's and Dan Cayan's involvement were facilitated by the U.S. Geological Survey Priority Ecosystems Study of the San Francisco Estuary.

Preface

The California Energy Commission's Public Interest Energy Research (PIER) Program supports public interest energy research and development that will help improve the quality of life in California by bringing environmentally safe, affordable, and reliable energy services and products to the marketplace.

The PIER Program conducts public interest research, development, and demonstration (RD&D) projects to benefit California's electricity and natural gas ratepayers. The PIER Program strives to conduct the most promising public interest energy research by partnering with RD&D entities, including individuals, businesses, utilities, and public or private research institutions.

PIER funding efforts focus on the following RD&D program areas:

- Buildings End-Use Energy Efficiency
- Energy-Related Environmental Research
- Energy Systems Integration
- Environmentally Preferred Advanced Generation
- Industrial/Agricultural/Water End-Use Energy Efficiency
- Renewable Energy Technologies
- Transportation

In 2003, the California Energy Commission's PIER Program established the **California Climate Change Center** to document climate change research relevant to the states. This center is a virtual organization with core research activities at Scripps Institution of Oceanography and the University of California, Berkeley, complemented by efforts at other research institutions. Priority research areas defined in PIER's five-year Climate Change Research Plan are: monitoring, analysis, and modeling of climate; analysis of options to reduce greenhouse gas emissions; assessment of physical impacts and of adaptation strategies; and analysis of the economic consequences of both climate change impacts and the efforts designed to reduce emissions.

The California Climate Change Center Report Series details ongoing center-sponsored research. As interim project results, the information contained in these reports may change; authors should be contacted for the most recent project results. By providing ready access to this timely research, the center seeks to inform the public and expand dissemination of climate change information, thereby leveraging collaborative efforts and increasing the benefits of this research to California's citizens, environment, and economy.

For more information on the PIER Program, please visit the Energy Commission's website www.energy.ca.gov/pier/ or contract the Energy Commission at (916) 654-5164.

Table of Contents

Preface.. iii
Abstract xi
1.0 Introduction 1
2.0 Climate Scenarios 1
3.0 Downscaling 6
4.0 Warming 6
5.0 Heat Waves 13
6.0 Precipitation 13
7.0 El Niño/Southern Oscillation 29
8.0 Sea Level Rise 30
9.0 North Pacific Wind Waves along the California Coast 36
10.0 Shore Zone Wave Runup Variability 40
11.0 Discussion 44
12.0 References 46
13.0 Glossary 49

List of Figures

Figure 1. California would retain its strong Mediterranean temperature and precipitation, as indicated by six GCMs, run under A2 (red) and B1 (blue) emission scenarios, along with historical simulated temperature and precipitation (black). Observed temperature and precipitation averages (1961–1990) from Sacramento are shown by gray symbols on the GFDL CM2.1 plot (middle). A2 temperature warming does not rise much above that of B1 by 2050. Temperature and precipitation have been taken directly from each GCM, no downscaling, from the grid point closest to Sacramento. 3

Figure 2. The global carbon emissions (gigatonnes of carbon, GtC) are shown by bars. The atmospheric CO_2 concentration (parts per million, volume, or ppmv) is shown by lines. The bars represent the historical period (black) and SRES B1 (blue) and SRES A2 (red) emissions scenarios. The black square represents the present day (2008) atmospheric concentration (386 ppmv). 5

Figure 3. Annual temperatures near Sacramento, for the six GCMs for 203CM simulations of the historical period (black) and for the projected 2000–2100 periods under the A2 (red) and B1 (blue) GHG emissions scenarios. In this case, the values plotted are taken directly from the GCMs from the grid point nearest to Sacramento. 8

Figure 4. Winter (January, February, March average, left) and summer (July, August, September average, right) surface air temperature changes for the Sacramento region, relative to each model's 1961–1990 average, for each of the six GCMs under the A2 (upper; red) and B1 (lower; blue) GHG emission scenarios. Sacramento region temperatures are extracted directly from each GCM from the grid point closest to Sacramento.....9

Figure 5. Spring temperature (°C) from the CNRM A2 simulation, for the historical and twenty-first century climate change periods. Years exceeding historical 90th percentile level (1961–1990) are shown in red. Temperature is for the Sacramento watershed, from Constructed Analogues downscaled CNRM data.....10

Figure 6. April 1 snow accumulation (snow water equivalent, SWE) from the CNRM A2 simulation. Years with less SWE than its historical 10th percentile (1961–1990) are shown in red. The 90th percentile and 10th percentile SWE levels are indicated by blue and black horizontal lines, respectively. SWE has been produced from Variable Infiltration Capacity (VIC) hydrological model driven by Constructed Analogues downscaled precipitation and temperature. 11

Figure 7. Amount of warming in July, (2045–2054 minus 1961–1990) and (2090–2099 minus 1961–1990) along a coast-to-interior transect for three GCMs under A2 simulation downscaled via Constructed Analogues to the region from San Francisco through the interior region of Central California. The transect is shown in the map at the lower right, which illustrates the amount of warming for July for the CNRM CM3 A2 simulation.....12

Figure 8. Number of days with simultaneous hot days (exceeding 95th percentile historical value) at nine key California locations, as projected by three GCMs, under B1 (left; blue) and A2 (right; red) GHG emission scenarios, using constructed analogues downscaling. Number of hot days from historical simulation shown by black bars.....16

Figure 9. Precipitation, by water year, 1901–1999 historical period (black) and 2000–2100 climate change period for SRES B1 (blue) and SRES A2 (red) GHG emission scenarios from six GCMs. The values plotted are taken directly from the GCMs from the grid point nearest to Sacramento.....17

Figure 10. Magnitude of year-to-year precipitation variability is very large in Southern California, as indicated by the ratio of the standard deviation to the mean precipitation (sigma/mean) for the water year. Historical and A2 simulations for three models are shown, along with estimated observed precipitation from NCEP Reanalysis 1. Magnitude of sigma/mean is indicated by dot size, and also by color assignment, shown by color key. The values plotted are taken directly from the GCMs. 18

Figure 11. Differences in 30-year mean annual total precipitation of early (2005–2034), middle (2035–2064), and late (2070–2099) twenty-first century relative to 1961–1990 climatology for each of six GCMs, for SRES B1 (lower; blue) and SRES A2 (upper; red). Precipitation is taken directly from the GCMs from the grid point nearest to Sacramento.....19

Figure 12. June soil moisture from the Variable Infiltration Capacity (VIC) hydrological model driven by the CNRM A2 simulation downscaled using the Constructed Analogues method. Years with soil moisture being less than historical 10th percentile level are shown in red.

The 90th percentile and 10th percentile June soil moisture levels are indicated by blue and black horizontal lines, respectively. 23

Figure 13. Simulated variability, in California sea level pressure index (CaSLP) (Cayan and Peterson 1989) for winter (upper) and spring (lower), shown in two right-hand side plots of 6 GCMs for 203CM historical simulations (black) and for B1 (blue) and A2 (red) emission scenario simulations. Maps on the left side show correlations of historical observed precipitation with NCEP Reanalysis sea level pressure, as indicated by contour lines, along with delineation of the 35-40°N, 125-135°W CaSLP "box." 25

Figure 14. Number of "storms" per year as indicated by days when average daily sea level pressure (SLP) is 1005 mb or less for historical (1950–2000) (black) and projected (2001–2100) periods of the three GCMs for the B1 (below; blue) and A2 (above; red) emissions scenarios. SLP is taken directly from GCMs for the grid point nearest San Francisco. 27

Figure 15. Number of days per year when precipitation at San Francisco equals or exceeds 25 mm. From constructed analogues downscaling of CNRM CM3, GFDL CM2.1, and NCAR PCM1 GCMs; result from BCSD downscaling (not shown) is very similar. Historical period and A2 2000–2100 projection indicated by black and red symbols, respectively. Precipitation is taken from BCSD downscaling. 29

Figure 16. Association of precipitation in San Diego region to ENSO, as indicated by the El Niño 3.4 sea surface temperature (SST) index, which is the area average sea surface temperature departure from the historical average in the central equatorial Pacific Ocean. Projected Niño 3.4 SST series have been adjusted by removing the linear trend to better discern interannual fluctuations. Precipitation values during cool, neutral, and warm Niño 3.4 SST years indicated by blue, green, and red dots respectively. San Diego region precipitation extracted directly from each of the GCMs, from the grid point nearest to San Diego. 31

Figure 17. Projected global sea level using the Rahmstorf (2007) scheme from each of the six models (set to zero at 2000). Climate change simulations for the SRES A1fi, A2 and B1 emission scenarios are shown for both the original Rahmstorf (dashed curves) and a version adjusted for the affect of reservoirs and dams (solid). Historical (black) and projected B1 simulations (blue), A2 simulations (red), A1fi (gold) are shown along with observed global sea level (aqua). 33

Figure 18. Hourly sea level simulated for San Francisco (Fort Point) location, using secular change estimated using the Rahmstorf (2007) scheme. Hourly sea level model from Cayan et al. 2008c includes this secular rise and superimposes predicted astronomical tides, barometric pressures winds, and ENSO from GFDL A2 simulation. Sea level values are referenced to the long-term mean historical average. 34

Figure 19. Maximum duration (hours) that San Francisco sea level, as depicted in Figure 18, exceeds the 99.99th percentile level (140 cm above mean sea level), as modeled from the GFDL historical (20C3M) simulation (black) and the GFDL climate change (SRESA2) simulation (red) using the Rahmstorf sea level scheme without adjustment for effect of dams.....35

Figure 20. The 99th percentile significant wave heights (Hs99), November through March for Reanalysis (purple), and CCSM A1 (green), CCSM A2 (red), and CNRM A2 climate simulations for Northern California coast offshore from San Francisco. Series have been smoothed with a 7-year running mean. 39

Figure 21. The 99th percentile significant wave heights (Hs99), November through March for Reanalysis (purple), and CCSM A1 (green), CCSM A2 (red), and CNRM A2 climate simulations for location offshore from Point Conception. Series have been smoothed with a 7-year running mean. 40

Figure 22. Winter (Nov.–Mar.) 99th percentiles of the WAVEWATCH III model significant wave height, *Hs*, projections forced by NCAR CCSM3 model winds. Offshore locations at northern California near Crescent City (CRE, 42ºN 126ºW; black), Central California near San Francisco (SFO, 38ºN 124.5ºW; red), and Southern California near San Miguel Island (SML, 34ºN 121.5ºW; green) are shown. Downward least squares trends steepen slightly going northward. These downward trends represent about a 9% decrease.....43

Figure 23. Projected mean winter (Nov.-Mar.) runup for the 98th percentile wave H_0 amplitudes for both low, B1 (red) and high, A2 (black) GHG emission scenario sea level projections. Low to moderate foreshore beach slopes, β, have upward trends with associated changes of 43%, 29%, and 16% for A2 and 31%, 20%, and 10% for B1 for β = 0.02, 0.05, 0.10, respectively. 44

List of Tables

Table 1. Heat waves, Sacramento area. Number of events in which daily maximum temperature (Tmax) exceeds historical (1961–1990) 95th percentile Tmax of May–September days. Events are counted separately for 1, 2, 3, 4, and 5 or more days in succession; these are mutually exclusive, e.g., a 1-day event does not include any 2, 3, 4, or 5 day events. Data used has been downscaled via Bias Corrected Spatial Downscaling. 15

Table 2. Evaluation of significance of differences in the SRES B1 (top) and SRES A2 (bottom) for the Shasta, Sacramento, and Los Angeles regions' 30-year mean precipitation from historical (1961–1900) average as a percent of historical annual average precipitation. Percentile ranks were obtained from placing 30-year average precipitation from each of the simulations within a distribution from a set of 1000 Monte Carlo sequences of the model historical precipitation. Values that are significant at the 95% confidence level are highlighted with bold type. Precipitation is taken directly from the GCMs from the grid point nearest Shasta, Sacramento, and Los Angeles, respectively. 20

Table 3. Trends 2000–2100 in the number of days when precipitation exceeds 3 mm (top), 15 mm (middle), and 25 mm (bottom) over the Shasta, Sacramento, and Los Angeles regions from SRES A2 simulations for CNRM, GFDL, and PCM GCMs, from grid points nearest these locations. Significance determined from Monte Carlo exercise generating distribution of 1000 possible historical trends. Values that are significant at the 95% confidence level are highlighted with bold type. 22

Table 4. North Pacific sea level pressure index (after Trenberth and Hurrell 1995), formed from average of November through March sea level pressure, 30N–65N, 160E–140W. Units are in hectopascals (hPa). 24

Table 5. California sea level pressure index, (after Cayan and Peterson 1989) formed from average of sea level pressure centered at 40N, 130W. Units are hPa. 26

Table 6. Trends in number of storms in the neighborhood of three regions: Crescent City, San Francisco, and La Jolla. *Storms* are defined as days having mean daily sea level pressure (SLP) less than 1005 mb in the neighborhood of Crescent City, San Francisco, or Shasta from the GCM (CNRM, GFDL, or CCSM). Percentile level of trend is indicated, as evaluated using a Monte Carlo sampling exercise. Values reaching the 90% level of significance are shown in boldface. 28

Table 7. Hourly Sea Level Exceedances, San Francisco. Number of hours and percent of total hours sea level exceeds the 99.99th historical (1960–1978) percentile for each 30 year period. The 99.99th historical percentile is 141 cm. 36

Table 8. Standard deviation of hourly sea level (cm) from the weather component of the sea level model 36

Table 9. Projected WWIII model significant wave height, *Hs*, percentile levels at Crescent City (CRE), San Francisco (SFO), and San Miguel Island (SML) over all 2000–2099 winters (November–March) 43

Abstract

For the 2008 California Climate Change Assessment, to further investigate possible future climate changes in California, a set of 12 climate change model simulations was selected and evaluated. From the Intergovernmental Panel on Climate Change Fourth Assessment activities projections, simulations of twenty-first century climates under a B1 (low emissions) and an A2 (a medium-high emissions) emissions scenarios were evaluated. Six climate models were chosen. These emission scenarios and climate simulations are not "predictions," but rather are possible scenarios of plausible climate sequences that might affect California in the next century. Temperatures over California warm significantly during the twenty-first century in each simulation. Also the rise in global sea level, and by extension the rise of sea level along the California coast, increases. Along with this, there are marked increases in the frequency, magnitude, and duration of heat waves and sea level rise extremes. There is quite a strong inclination for higher warming in summer than winter and greater warming inland than along the coast. In several of the simulations there is a tendency for drier conditions to develop during mid-and late-twenty-first century in Central and Southern California, and along with this, a decline in winter wave energy along the California coast.

Keywords: Regional climate change, California, hydroclimate adaptation, sea level rise, waves, runup

1.0 Introduction

This is a contribution to the second California Climate Change Scenarios Assessment. The assessment process has its origin in an Executive Order S-3-05, which, in addition to setting greenhouse gas emission targets, charges the Secretary of the California Environmental Protection Agency to "report to the Governor and the State Legislature by January 2006 and biannually thereafter on the impacts to California of global warming."

This work is motivated by recent examinations of observed climate in California and the western United States that have demonstrated that recent warming and associated hydrological changes are unlikely to have been caused entirely by natural climate fluctuations (Bonfils et al. 2007; Maurer et al. 2007). Furthermore, subsequent studies (Barnett et al. 2008; Pierce et al. 2008; Bonfils et al. 2008) demonstrated that it is very likely that major parts of these changes were caused by greenhouse gas loading of the atmosphere by humans. The present study builds upon previous climate model-based studies of possible climate change impacts on various sectors in the California region, including a broad assessment of possible ecological impacts by Field et al. (1999); an assessment of a range of potential climate changes on ecosystems, health, and economy in California described by Wilson et al. (2003); a study of how a "business-as-usual emissions scenario simulated by a low sensitivity climate model would affect water resources in the western United States, overviewed by Barnett et al. (2004); a multisectoral assessment of the difference in impacts arising from high versus low greenhouse gas (GHG) emissions in Hayhoe et al. (2004); and the initial 2006 California climate change scenarios assessments (e.g., Franco et al. 2008; Cayan et al. 2008a; Cayan et al. 2008b).

2.0 Climate Scenarios

In view of the uncertainty in the climate responses by greenhouse gases and other forcings and the variability amongst models in representing and calculating key processes, it is important to consider results from several climate models rather than to rely on just a few. For the 2008 California Climate Change Scenarios Assessment, the set of global climate models (GCMs) evaluated has been expanded to GCMs that contributed to the recent Intergovernmental Panel on Climate Change (IPCC) Fourth Assessment (IPCC 2007) using *Special Report on Emissions Scenarios* (SRES) A2 and B1 emission scenarios were employed to assess climate changes and their impacts.

The following models were selected for the assessment: the National Center for Atmospheric Research (NCAR) Parallel Climate Model (PCM); the National Oceanic and Atmospheric Administration (NOAA) Geophysical Fluids Dynamics Laboratory (GFDL) model, version 2.1; the NCAR Community Climate System Model (CCSM); the Max Plank Institute ECHAM5/MPI-OM; the MIROC 3.2 medium-resolution model from the Center for Climate System Research of the University of Tokyo and collaborators; and the French Centre National de Recherches Météorologiques (CNRM) models.

These models, only a subset of those included in the IPCC Fourth Assessment, were selected on the basis of providing a set of relevant monthly, and in some cases daily, data. Another rationale was that the models provided a reasonable representation, from their historical simulation, of the following elements: seasonal precipitation and temperature (Figure 1), the variability of annual precipitation, and El Niño/Southern Oscillation (ENSO). It should be

noted though, that the historical skill criteria is probably not very well founded, since it has been shown that model historical skill is not well related to model climate change performance (Coquard et al. 2004; Brekke et al. 2008). The emission scenarios considered are among the same ones that were used for the 2006 California climate change scenarios Assessment (Cayan et al. 2008). The A2 emissions scenario represents a differentiated world in which economic growth is uneven and the income gap remains large between now-industrialized and developing parts of the world, and people, ideas, and capital are less mobile so that technology diffuses more slowly. The B1 emissions scenario presents a future with a high level of environmental and social consciousness, combined with a globally coherent approach to a more sustainable development (Figure 2). To put the A2 and B1 scenarios into perspective, however, it is worth noting that the estimated emissions growth for 2000–2007 was above even the most fossil fuel intensive scenario of the Intergovernmental Panel on Climate Change (SRES-IPCC) (Science Daily 2008).

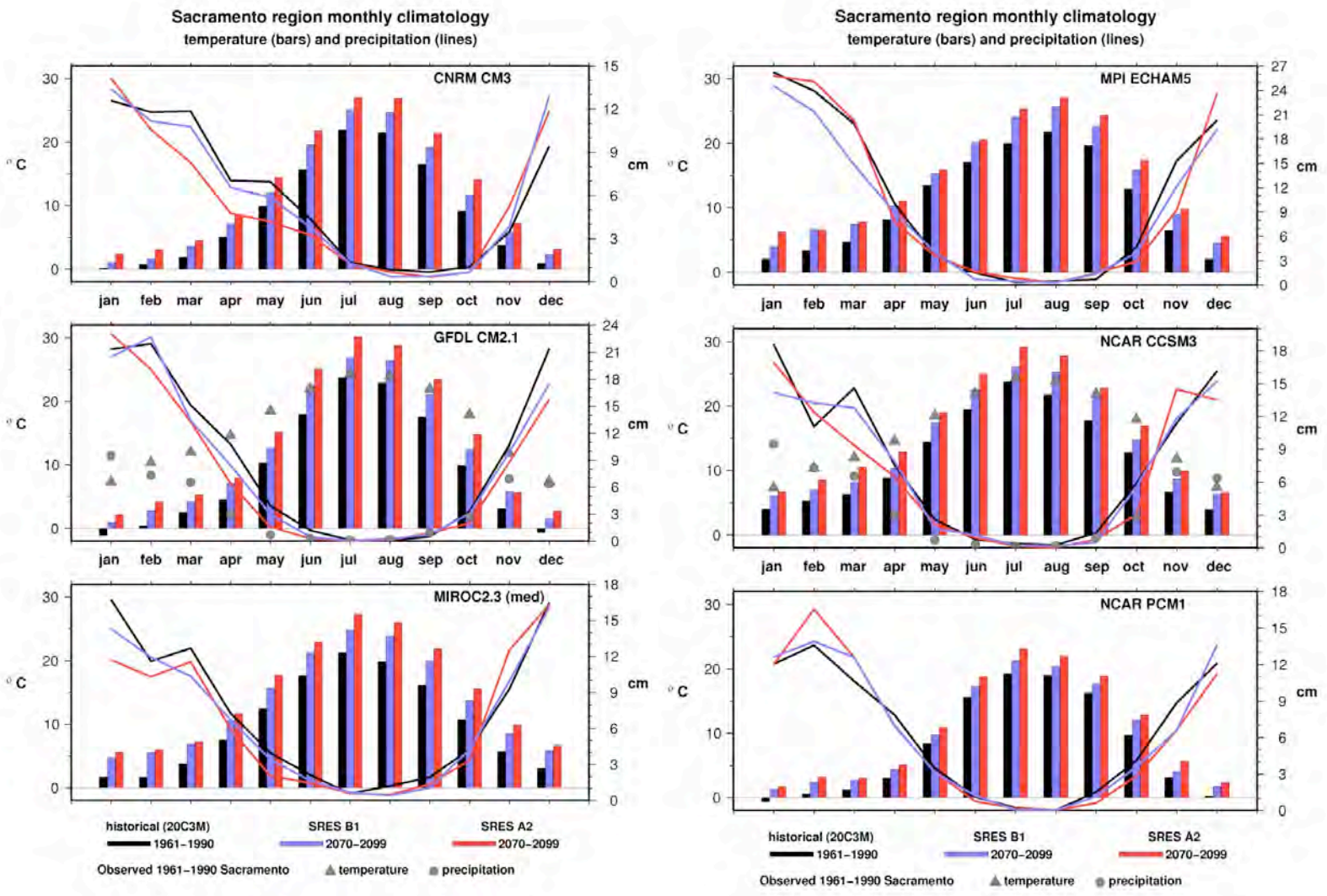

Figure 1. California would retain its strong Mediterranean temperature and precipitation, as indicated by six GCMs, run under A2 (red) and B1 (blue) emission scenarios, along with historical simulated temperature and precipitation (black). Observed temperature and precipitation averages (1961–1990) from Sacramento are shown by gray symbols on the GFDL CM2.1 plot (middle). A2 temperature warming does not rise much above that of B1 by 2050.

Temperature and precipitation have been taken directly from each GCM, no downscaling, from the grid point closest to Sacramento.

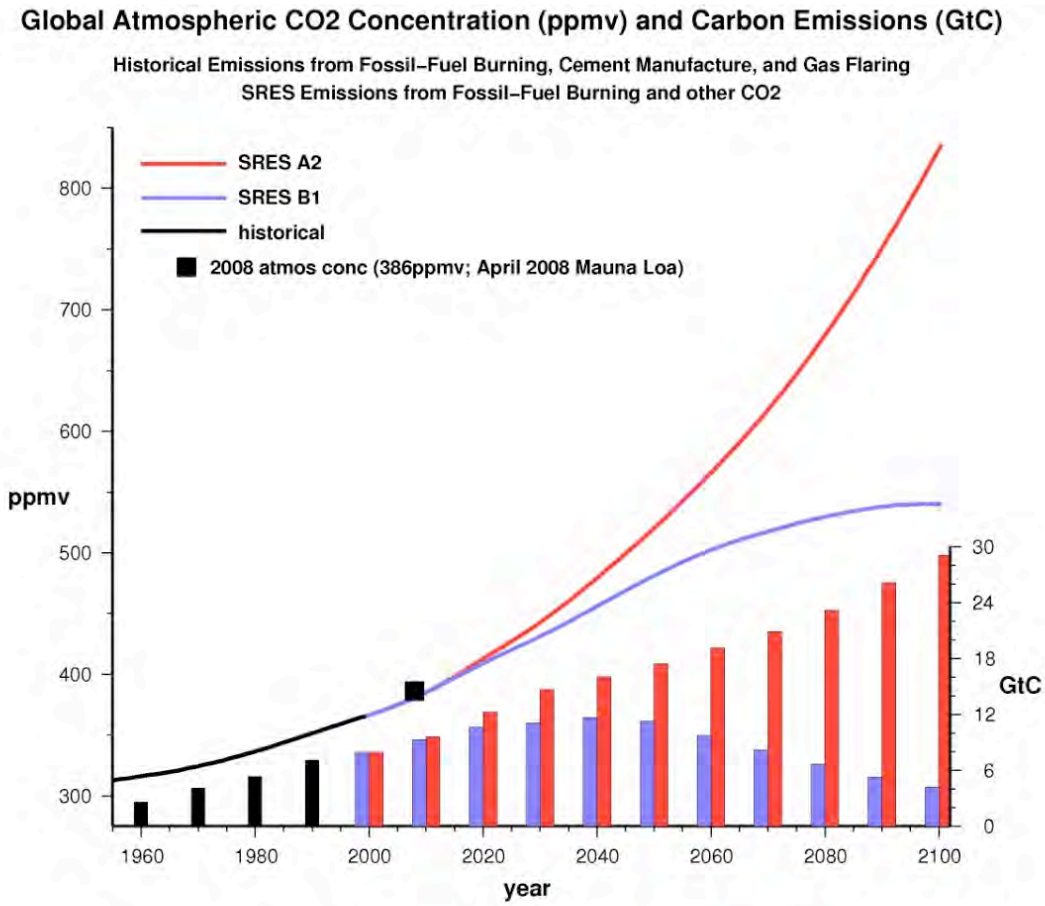

Figure 2. The global carbon emissions (gigatonnes of carbon, GtC) are shown by bars. The atmospheric CO_2 concentration (parts per million, volume, or ppmv) is shown by lines. The bars represent the historical period (black) and SRES B1 (blue) and SRES A2 (red) emissions scenarios. The black square represents the present day (2008) atmospheric concentration (386 ppmv).

Because there is considerable uncertainty in future greenhouse gas emissions, it is not possible to assign odds to either of the two emissions scenarios. Also, each GCM differs, to some extent, in its representation of various physical processes from other GCMs, and so the different models contain different levels of warming, different patterns and changes of precipitation, and so on. The result is a set of model simulations having different climate characteristics, even when the models are driven by the same GHG emissions scenario. Consequently, the climate projections should be viewed as a set of possible outcomes, each having an unspecified degree of uncertainty. In short, these models results provide a rather coarse set of scenarios from which to view the future; but they are not detailed predictions.

As has been emphasized in the IPCC results and in prior California climate change assessments, results of different mitigation strategies, as expressed by the two GHG emission scenarios (A2 medium-high emissions and B1 moderately low emissions) do not become very clear until after the middle of the twenty-first century—they are much more distinctly evident in the following decades (IPCC 2007; Hayhoe et al. 2004; Cayan et al. 2008).

3.0 Downscaling

The two downscaling methods employed in the 2009 California Assessment are (1) constructed analogues (CA), and (2) bias correction and spatial downscaling (BCSD). Maurer and Hidalgo (2008) compare the two methods and find that they both perform reasonably well, but they do contain some noteworthy differences. Both methods have been shown to be skillful in different settings, and BCSD (Wood et al. 2004) has been used extensively in hydrologic impact analysis. Both methods use the coarse scale Reanalysis fields of precipitation and temperature as predictors of the corresponding fine scale fields. The CA (Hidalgo et al. 2008) method downscales daily large-scale data directly, and BCSD downscales monthly data, with a random resampling technique to generate daily values. The methods produce generally comparable skill in producing downscaled, gridded fields of precipitation and temperatures at a monthly and seasonal level. For daily precipitation, both methods exhibit limited skill in reproducing both observed wet and dry extremes, and the difference between the methods is not significant, reflecting the general low skill in daily precipitation variability in the reanalysis data. For low temperature extremes, the CA method produces greater downscaling skill than BCSD for fall and winter seasons. For high temperature extremes, CA demonstrates higher skill than BCSD in summer. The most appropriate downscaling technique depends on the variables, seasons, and regions of interest; on the availability of daily data; and whether the day-to-day correspondence of weather from the GCM needs to be reproduced for some applications. The ability to produce skillful downscaled daily data depends primarily on the ability of the climate model to show daily skill. In the selected examples shown here, we employ results using either the BCSD or the CA method. Most of the cases which we have compared have yielded comparable results, but the degree of similarity varies depending on the topic, with cases that feature rarer individual events having the greatest likelihood for substantial difference between the two.

4.0 Warming

From observed climate and hydrologic records and from the model historical simulations, it is seen that the model simulations begin to warm more substantially in the 1970s; this is likely a

response to effects of GHG increases, which began to increase significantly during this time period (Bonfils et al. 2007; Barnett et al. 2008).

All of the climate model simulations exhibit warming, globally and regionally over California (Figure 1 and Figure 3). In the early part of the twenty-first century, the amount of warming produced by the A2 scenario is not too much greater than that of B1, but becomes increasing larger through the middle and especially the latter part of the century (Figure 3 and Figure 4). Overall, the six models' warming projections in mid-century range from about 1°C to 3°C (1.8°F to 5.4°F), rising by end-of-twenty-first century, from about 2°C to 5°C (3.6°F to 9°F). The upper part of this range is a considerably greater warming rate than the historical rates estimated from observed temperature records in California (Bonfils et al. 2008).

There is considerable variability between the six GCMs, but the lower sensitivity model (the PCM) contains the lowest temperature rise in both cool and warm seasons. The models do contain decade-to-decade variability, but this decadal component is not too large, and overall there is a steady, rather linear increase over the 2000–2100 period (Figure 3). All of the model runs result in a loss of spring snowpack in California, as has been previously discussed (e.g., Hayhoe et al. 2004; Cayan et al. 2008b). The models produce substantial warming during the hydrologically sensitive spring period (Figure 5). Along with the increasing occurrence of very warm spring temperatures, a sensitive index of the spring snow loss is the increasingly frequent incidence of tenth percentile snow years, illustrated for the CNRM A2 model run in Figure 6.

There is considerable asymmetry, both seasonally and spatially, in the amount of warming (Figure 4). Winter (January–March) temperature changes range from 1°C–4°C (1.8°F–7.2°F) in the six GCMs, under A2 and B1 GHG emissions scenarios, averaged over 30 years at the end of the twenty-first century relative to the 1961–1990 climatology. Importantly, there is greater warming in summer than in winter. Summer (July–September) temperature changes range from 1.5°C–6°C (2.7°F–10.8°F) over the six GCMs, under A2 and B1 GHG emissions scenarios. During summer, the models suggest that climate warming of land surface temperatures is amplified in the interior of the California as shown by the temperature change along a coast-interior transect through the San Francisco Bay region (Figure 7). A distinct Pacific Ocean influence occurs, wherein warming is more moderate in the zone of about 50 kilometers (km) from the coast, but rises considerably, as much as 4°C (7.2°F) higher, in the interior landward areas as compared to the warming that occurs right along the coast.

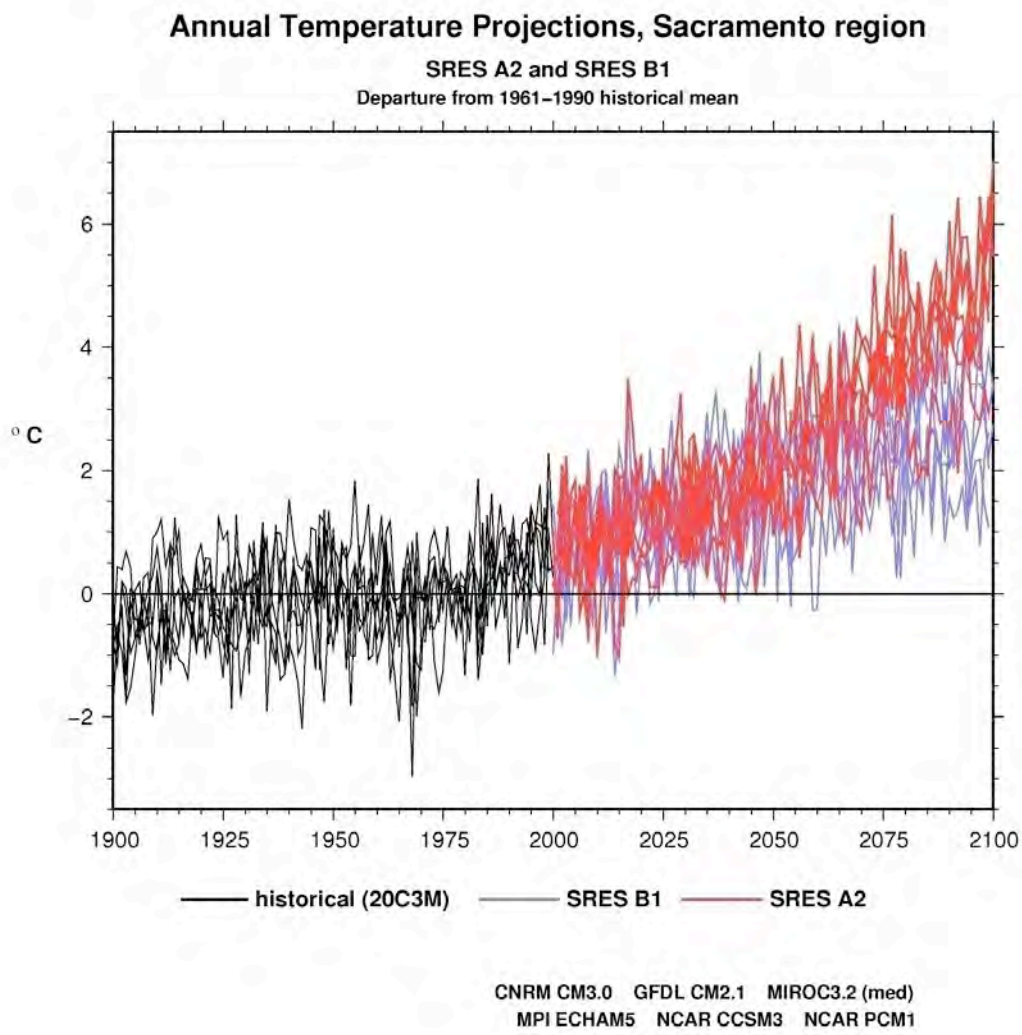

Figure 3. Annual temperatures near Sacramento, for the six GCMs for 203CM simulations of the historical period (black) and for the projected 2000–2100 periods under the A2 (red) and B1 (blue) GHG emissions scenarios. In this case, the values plotted are taken directly from the GCMs from the grid point nearest to Sacramento.

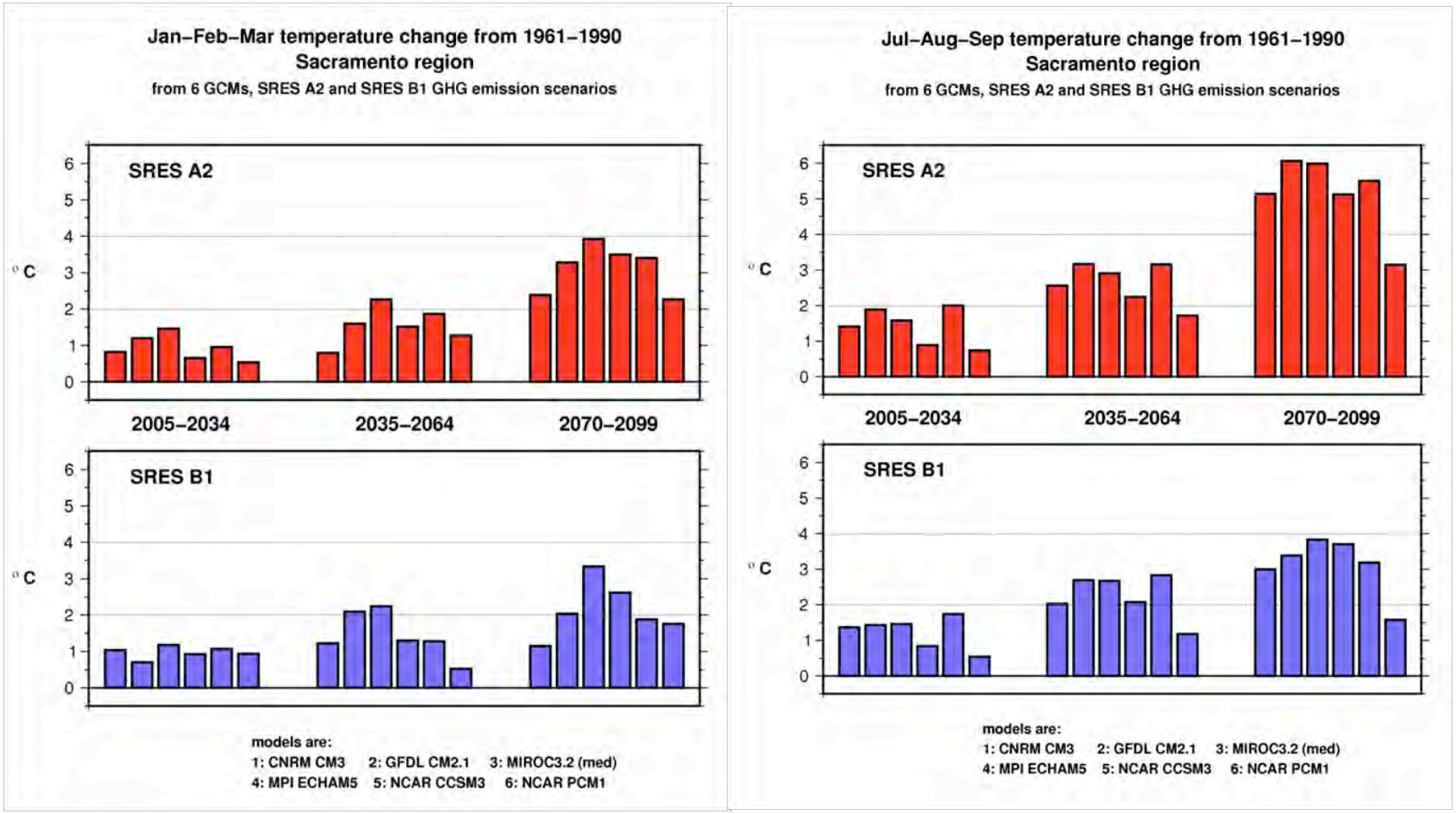

Figure 4. Winter (January, February, March average, left) and summer (July, August, September average, right) surface air temperature changes for the Sacramento region, relative to each model's 1961–1990 average, for each of the six GCMs under the A2 (upper; red) and B1 (lower; blue) GHG emission scenarios. Sacramento region temperatures are extracted directly from each GCM from the grid point closest to Sacramento.

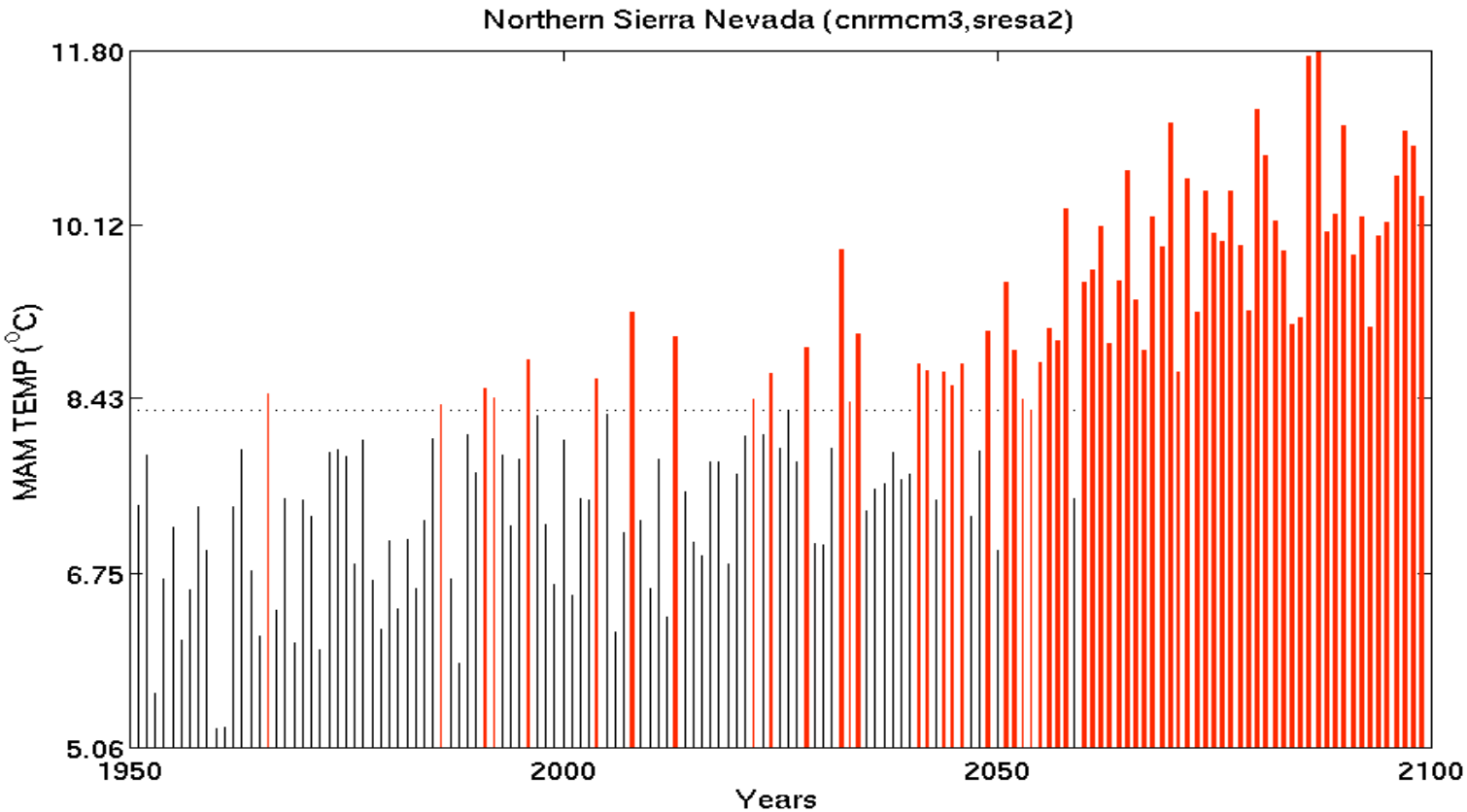

Northern California spring temperature CNRM A2

Figure 5. Spring temperature (°C) from the CNRM A2 simulation, for the historical and twenty-first century climate change periods. Years exceeding historical 90th percentile level (1961–1990) are shown in red. Temperature is for the Sacramento watershed, from Constructed Analogues downscaled CNRM data.

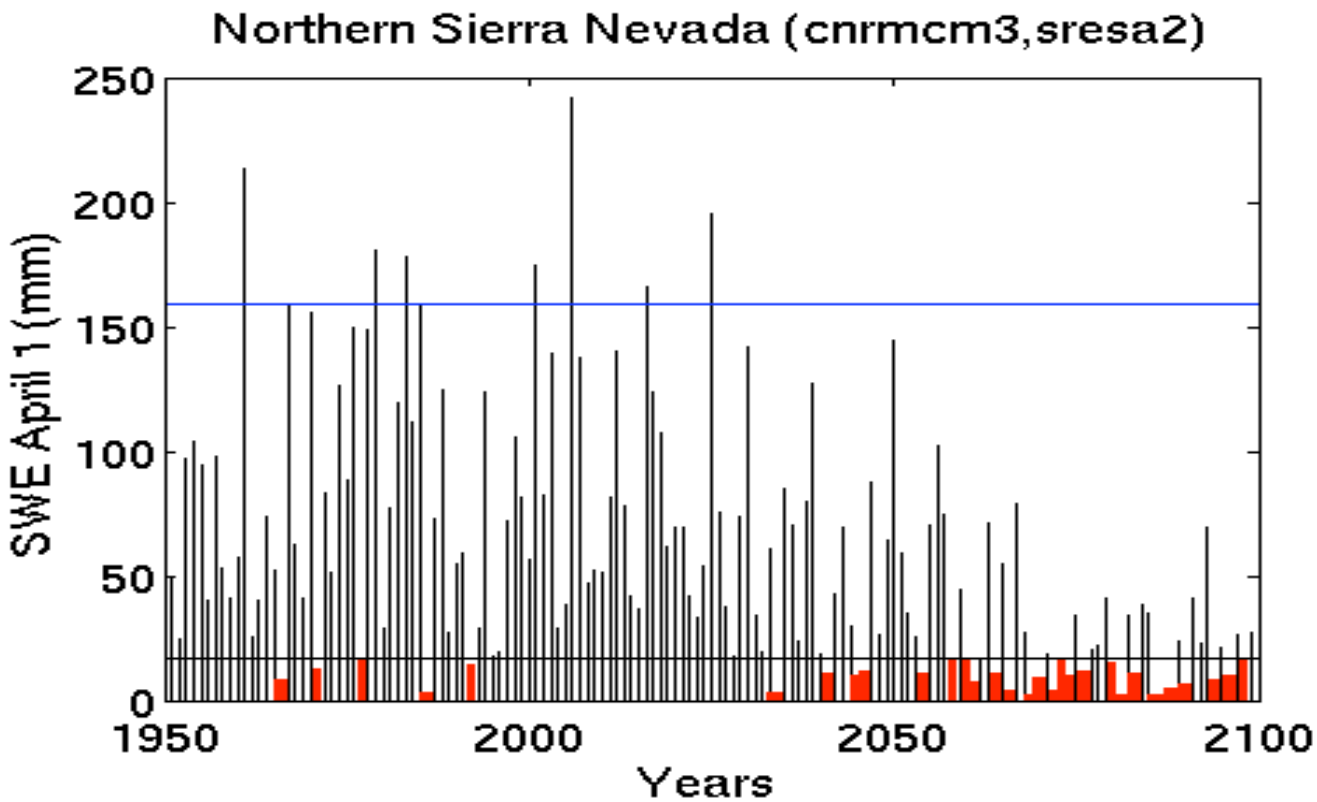

Snow Accumulation (April 1) CNRM

Figure 6. April 1 snow accumulation (snow water equivalent, SWE) from the CNRM A2 simulation. Years with less SWE than its historical 10th percentile (1961–1990) are shown in red. The 90th percentile and 10th percentile SWE levels are indicated by blue and black horizontal lines, respectively. SWE has been produced from Variable Infiltration Capacity (VIC) hydrological model driven by Constructed Analogues downscaled precipitation and temperature.

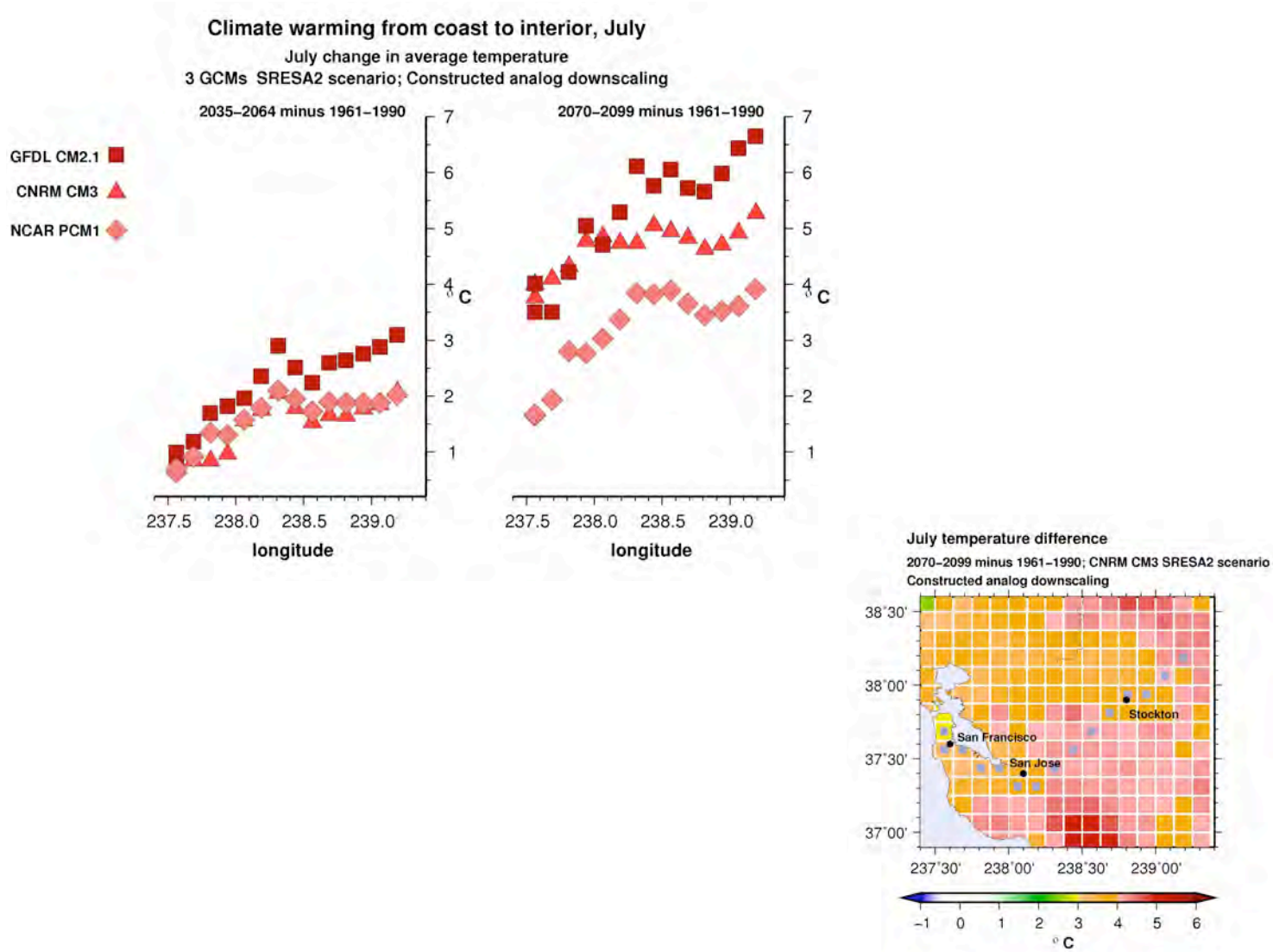

Figure 7. Amount of warming in July, (2045–2054 minus 1961–1990) and (2090–2099 minus 1961–1990) along a coast-to-interior transect for three GCMs under A2 simulation downscaled via Constructed Analogues to the region from San Francisco through the interior region of Central California. The transect is shown in the map at the lower right, which illustrates the amount of warming for July for the CNRM CM3 A2 simulation.

5.0 Heat Waves

Historically, extreme warm temperatures in the California region have mostly occurred in July and August (Gershunov and Cayan 2008), but as climate warming takes hold, the occurrences of these events will increase in frequency and magnitude (Hayhoe et al. 2004; Gershunov and Douville 2008; Miller et al. 2008) and likely will begin in June and could continue to be found in September. All simulations indicate that hot daytime and nighttime temperatures (heat waves) increase in frequency, magnitude, and duration from the historical period and during the projected period through the first half of the twenty-first century (Table 1). Several model simulations for a location near Sacramento contain a more-than-threefold increase in frequency and a decided increase in intensity of hot days. Within a given heat wave, there is an increasing tendency for multiple hot days in succession, and the spatial footprint of heat waves is more and more likely to encompass multiple population centers in California. Figure 8 depicts the number of hot days that occur concurrently at successively larger spatial scales within California, as represented by collectives of key stations as defined by the California Energy Commission. Also, as cataloged in Table 1, the duration of heat waves tends to grow longer through the twenty-first century as "average" conditions warm. Especially important is the occurrence of events having durations of five days or longer, which become much more prevalent—20 times or more frequent in several of the simulations—by the last 30 years of the twenty-first century.

6.0 Precipitation

Precipitation in most of California is characterized by a strong Mediterranean pattern wherein most of the annual precipitation falls in the cooler part of the year between November and March. The climate change simulations from these GCMs indicate that California will retain its Mediterranean climate with relatively cool and wet winters and hot dry summers (Figure 1). Another important aspect of the precipitation climatology is the large amount of variability, not only from month to month but from year to year and decade to decade (Figure 9). This variability stands out when mapped across the North Pacific and western North America complex, and it is quite well represented by models in comparison to the observed level of variability from global atmospheric data, via the NOAA National Centers for Environmental Prediction (NCEP) Reanalysis. The climate model-projected simulations indicate that the high degree of variability of annual precipitation will also prevail during the next century (Figure 10), which would suggest that the region will remain vulnerable to drought. The examples presented here, oriented on Sacramento, do not capture the magnitude of precipitation in the heaviest key watersheds in California. However, because winter precipitation in Sacramento is well correlated to that in the Sierra Nevada, these measures are representative of precipitation variability in the watersheds of the central Sierra Nevada and coast regions.

But in addition to the interannual-decadal variability contained within the simulations, there is a decided drying tendency (Figures 9 and 11). By mid- and late-twenty-first century, all but one of the simulations has declined relative to its historical (1961–1990) average. For the B1 simulation in mid-twenty-first century, two of the six simulations have a 30-year mean precipitation in Sacramento that is more than 5% drier than its historical average, and by late-twenty-first century, three of the six have 30-year averages that decline to more than 10% below their historical average. By the late twenty-first century, the differences of 30-year mean

precipitation from its historical average in three of the B1 simulations and four of the A2 simulations reaches a magnitude exceeding the 95% confidence level, as gauged from a Monte Carlo exercise that establishes the distribution of a historical sample, shown in Table 2. By the mid- and late-twenty-first century, only one of the simulations has 30-year mean precipitation that is wetter (slightly) than the historical annual average. Also shown in Table 2, the 30-year mean precipitation changes are similar in the southern part of the state, in the Los Angeles region, but not as consistent in the far northern part of the state, in the Shasta region. Consideration of the projected sequence of daily precipitation events indicates that the drying of annual precipitation in three of the models is associated with both a decline in the *frequency* of precipitation events but not a clear cut change in precipitation *intensity*. These changes are indicated (Table 3) by three of the models having downward trends in the number of 3 millimeter (mm) and greater daily precipitation events (e.g., the frequency of most of the precipitation events that occur) in each of the Shasta, Sacramento, and Los Angeles regions. Changes in frequency of days with heavier (15 mm and greater, and 25 mm and greater) precipitation events was not as consistent as the changes in broader category of 3 mm and greater days, indicating that the rarer, heavy events may be dictated by processes that do not necessarily mimic the more general trends.

Even for a simulation whose mean precipitation is essentially unchanged, in this case the CNRM A2 run, the warming alone would not only deplete the spring snowpack but accentuate the summer dryness, as determined by Variable Infiltration Capacity (VIC) hydrological model calculations of soil moisture in the Central California region (Figure 12).

Table 1. Heat waves, Sacramento area. Number of events in which daily maximum temperature (Tmax) exceeds historical (1961–1990) 95th percentile Tmax of May–September days. Events are counted separately for 1, 2, 3, 4, and 5 or more days in succession; these are mutually exclusive, e.g., a 1-day event does not include any 2, 3, 4, or 5 day events. Data used has been downscaled via Bias Corrected Spatial Downscaling.

GCM/simulation	30-yr period	1 day	2 days	3 days	4 days	5 or more days	Total days (of 4590)
CNRM CM3 SRESA2	1961–1990	37	20	23	16	3	232
	2005–2034	44	15	37	30	13	384
	2035–2064	56	33	36	30	23	495
	2070–2099	104	48	56	24	66	975
SRESB1	1961–1990	29	25	23	18	2	233
	2005–2034	45	27	28	32	11	378
	2035–2064	54	24	29	37	17	445
	2070–2099	70	25	36	33	30	550
GFDL CM2.1 SRESA2	1961–1990	40	24	28	7	5	231
	2005–2034	91	45	37	34	23	588
	2035–2064	149	60	46	42	46	941
	2070–2099	91	76	39	36	132	1747
SRESB1	1961–1990	29	26	25	17	1	231
	2005–2034	62	29	26	42	12	445
	2035–2064	71	30	37	28	35	583
	2070–2099	94	56	40	26	48	748
MIROC3.2 (med) SRESA2	1961–1990	39	22	29	14	1	231
	2005–2034	52	26	41	30	16	461
	2035–2064	75	26	49	27	49	723
	2070–2099	84	64	50	49	83	1352
SRESB1	1961–1990	40	27	25	14	2	233
	2005–2034	47	27	28	34	15	413
	2035–2064	80	38	35	28	34	606
	2070–2099	113	55	41	18	62	835

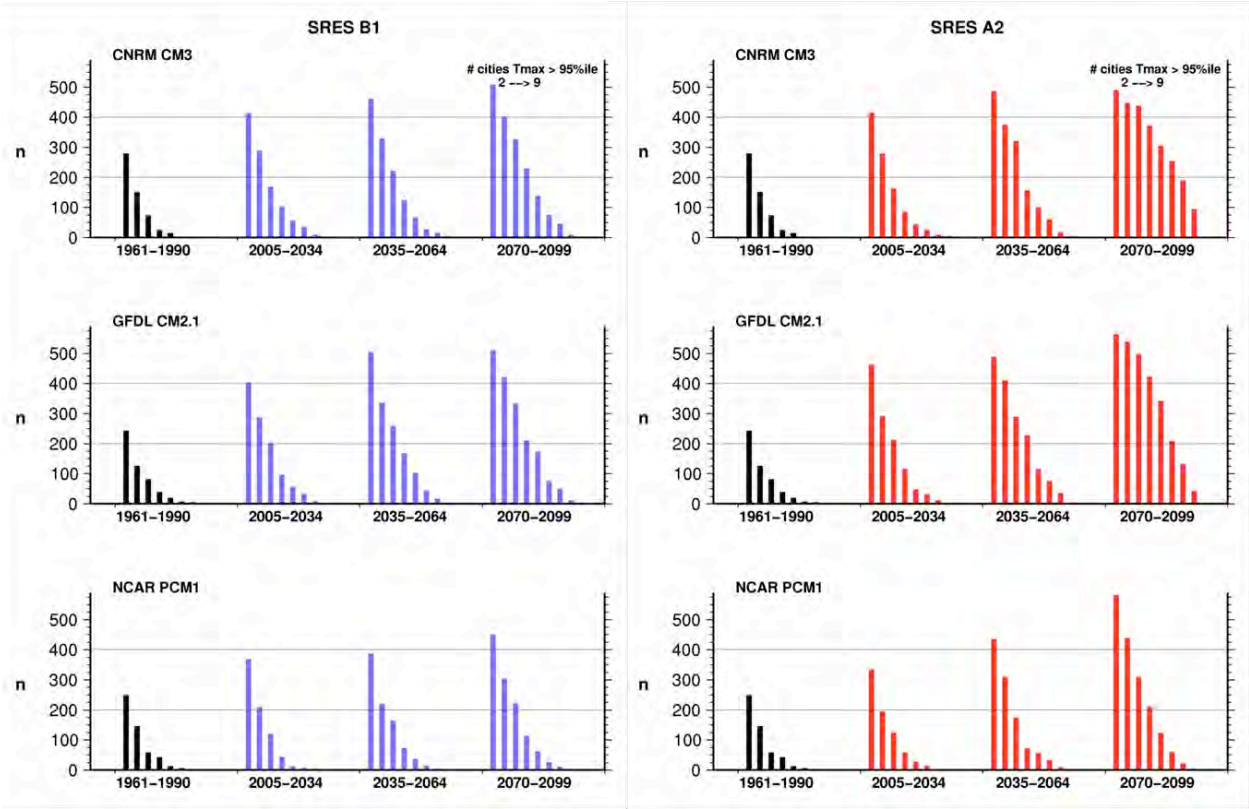

Figure 8. Number of days with simultaneous hot days (exceeding 95th percentile historical value) at nine key California locations, as projected by three GCMs, under B1 (left; blue) and A2 (right; red) GHG emission scenarios, using constructed analogues downscaling. Number of hot days from historical simulation shown by black bars.

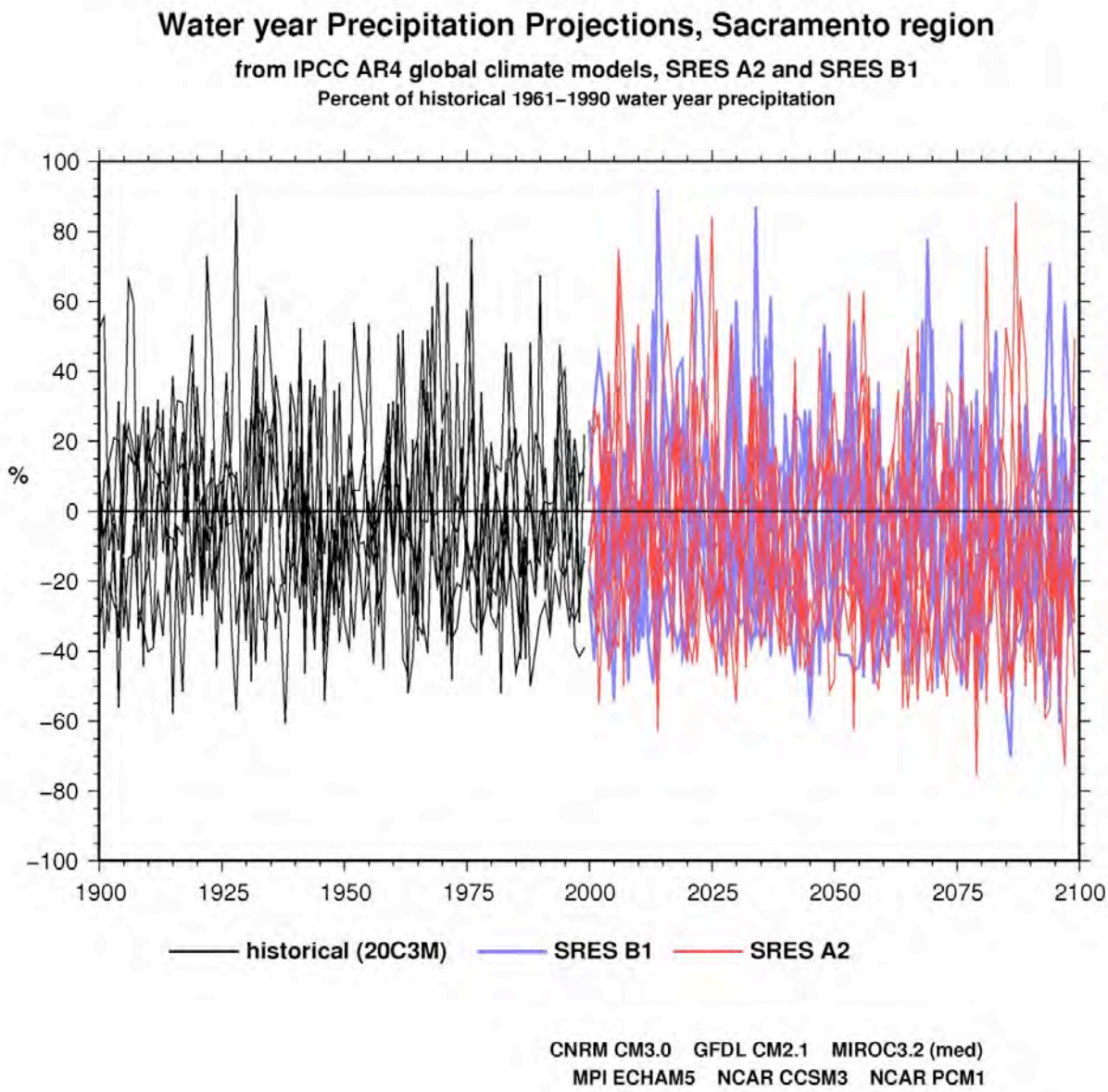

Figure 9. Precipitation, by water year, 1901–1999 historical period (black) and 2000–2100 climate change period for SRES B1 (blue) and SRES A2 (red) GHG emission scenarios from six GCMs. The values plotted are taken directly from the GCMs from the grid point nearest to Sacramento.

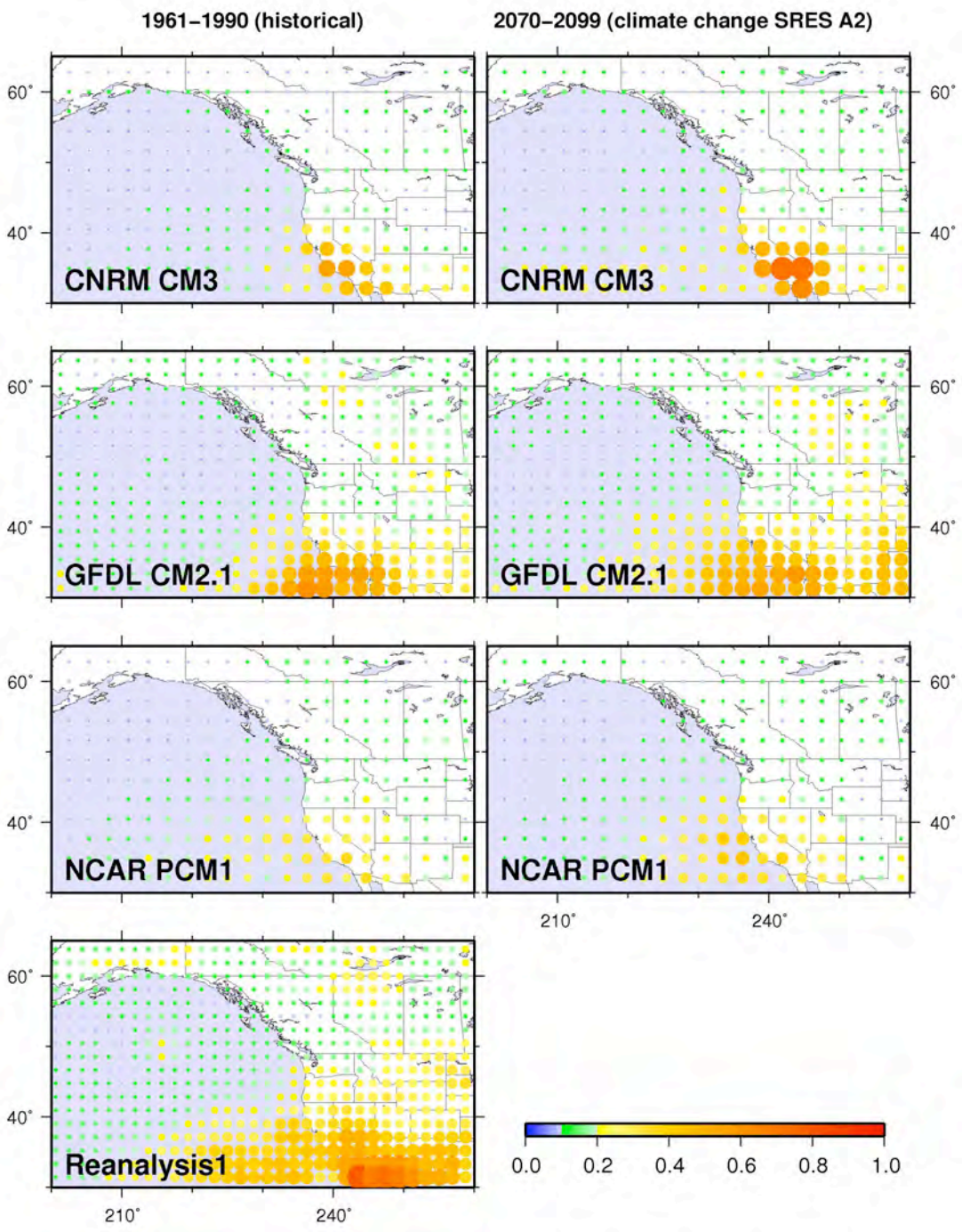

Figure 10. Magnitude of year-to-year precipitation variability is very large in Southern California, as indicated by the ratio of the standard deviation to the mean precipitation (sigma/mean) for the water year. Historical and A2 simulations for three models are shown, along with estimated observed precipitation from NCEP Reanalysis 1. Magnitude of sigma/mean is indicated by dot size, and also by color assignment, shown by color key. The values plotted are taken directly from the GCMs.

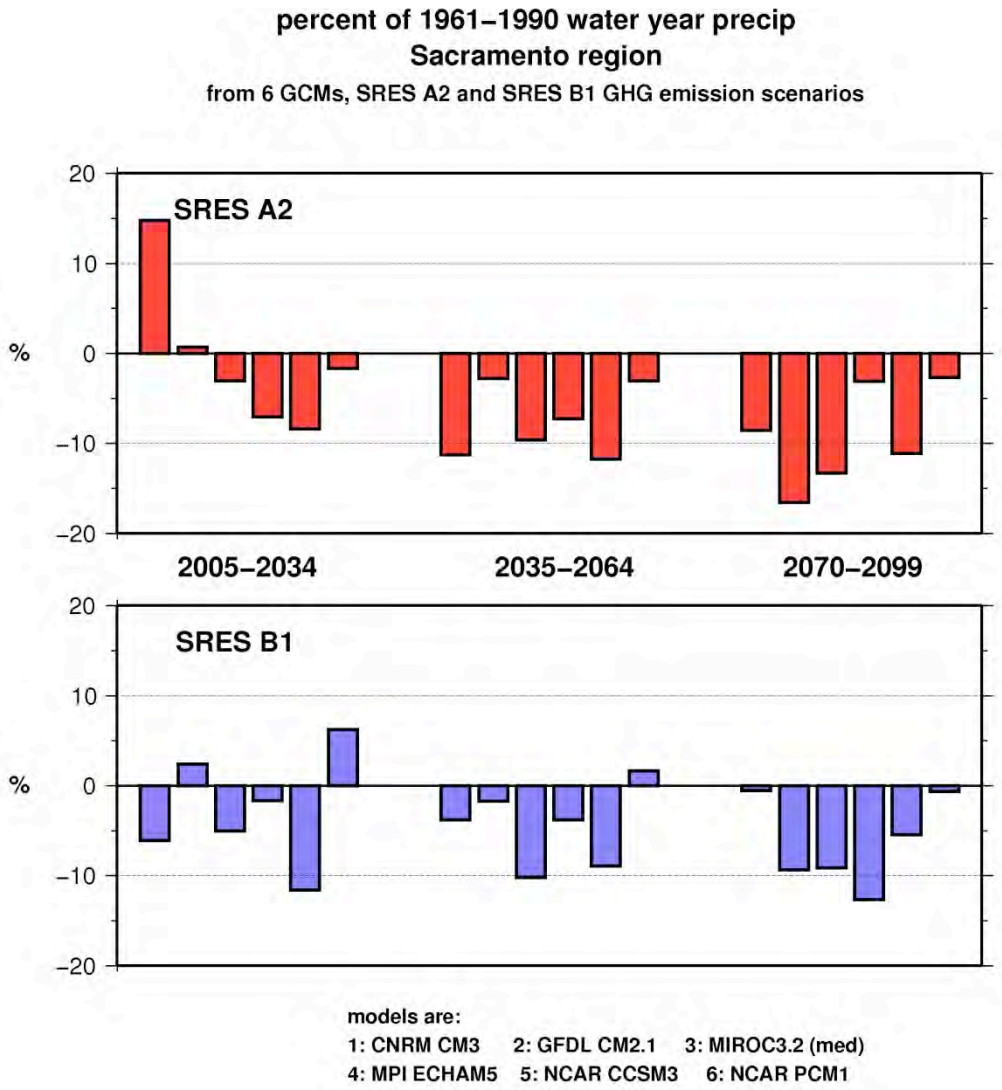

Figure 11. Differences in 30-year mean annual total precipitation of early (2005–2034), middle (2035–2064), and late (2070–2099) twenty-first century relative to 1961–1990 climatology for each of six GCMs, for SRES B1 (lower; blue) and SRES A2 (upper; red). Precipitation is taken directly from the GCMs from the grid point nearest to Sacramento.

Table 2. Evaluation of significance of differences in the SRES B1 (top) and SRES A2 (bottom) for the Shasta, Sacramento, and Los Angeles regions' 30-year mean precipitation from historical (1961–1900) average as a percent of historical annual average precipitation. Percentile ranks were obtained from placing 30-year average precipitation from each of the simulations within a distribution from a set of 1000 Monte Carlo sequences of the model historical precipitation. Values that are significant at the 95% confidence level are highlighted with bold type. Precipitation is taken directly from the GCMs from the grid point nearest Shasta, Sacramento, and Los Angeles, respectively.

Shasta SRES B1

Model	2005–2034	Rank (%)	2035–2064	Rank (%)	2070–2099	Rank (%)
CNRM CM3	+0.03	34	+4.41	89	**+7.45**	**99**
GFDL CM2.1	+2.83	45	+0.19	16	**-3.73**	**1**
MIROC3.2 (med)	-0.32	26	-2.07	11	+0.69	38
MPI ECHAM5	-2.13	18	-0.74	32	**-5.91**	**1**
NCAR CCSM3	**-10.35**	**1**	**-7.91**	**4**	-6.94	7
NCAR PCM1	+4.06	85	+4.27	87	+1.76	62

Sacramento SRES B1

Model	2005–2034	Rank (%)	2035–2064	Rank (%)	2070–2099	Rank (%)
CNRM CM3	-6.07	8	-3.77	17	-0.53	39
GFDL CM2.1	+2.42	51	-1.72	17	**-9.32**	**0.3**
MIROC3.2 (med)	-5.01	12	**-10.17**	**0.2**	**-9.11**	**0.4**
MPI ECHAM5	-1.64	31	-3.79	14	**-12.65**	**0.1**
NCAR CCSM3	**-11.60**	**1**	**-8.89**	**4**	-5.43	20
NCAR PCM1	+6.22	89	+1.65	52	-0.65	28

Los Angeles SRES B1

Model	2005–2034	Rank (%)	2035–2064	Rank (%)	2070–2099	Rank (%)
CNRM CM3	**-14.96**	**4**	**-24.76**	**0.1**	**-23.15**	**0.1**
GFDL CM2.1	-2.14	31	**-11.62**	**3**	**-22.59**	**0.1**
MIROC3.2 (med)	-18.40	11	**-24.64**	**0.3**	**-35.93**	**0.1**
MPI ECHAM5	-3.84	54	-4.00	54	**-16.35**	**1**
NCAR CCSM3	**-8.07**	**0.4**	+12.54	77	-1.13	8
NCAR PCM1	+16.96	94	**-2.81**	**3**	+7.18	45

Table 2. (continued)

Shasta SRES A2

Model	2005–2034	Rank (%)	2035–2064	Rank (%)	2070–2099	Rank (%)
CNRM CM3	**+9.75**	**99**	+0.03	34	+1.90	60
GFDL CM2.1	-0.57	11	**-5.23**	**0.3**	**-13.12**	**0.1**
MIROC3.2 (med)	+1.02	43	-1.07	18	-0.70	21
MPI ECHAM5	-3.42	9	-0.99	29	-1.09	27
NCAR CCSM3	**-20.81**	**0.1**	**-23.35**	**0.1**	**-23.3**	**0.1**
NCAR PCM1	+0.04	41	+1.53	59	-3.36	8

Sacramento SRES A2

Model	2005–2034	Rank (%)	2035–2064	Rank (%)	2070–2099	Rank (%)
CNRM CM3	**+14.79**	**99**	**-11.24**	**0.6**	**-8.51**	**2**
GFDL CM2.1	+0.68	35	-2.78	12	**-16.56**	**0.1**
MIROC3.2 (med)	-3.02	24	**-9.61**	**0.3**	**-13.28**	**0.1**
MPI ECHAM5	-7.05	**2**	**-7.27**	**1**	-3.07	19
NCAR CCSM3	-8.37	6	**-11.73**	**1**	**-11.09**	**1**
NCAR PCM1	-1.68	20	-3.06	12	-2.69	13

Los Angeles SRES A2

Model	2005–2034	Rank (%)	2035–2064	Rank (%)	2070–2099	Rank (%)
CNRM CM3	**+21.23**	**98**	**-41.10**	**0.1**	**-22.96**	**0.1**
GFDL CM2.1	-6.38	12	-2.48	29	**-25.77**	**0.1**
MIROC3.2 (med)	-19.48	7	**-30.09**	**0.1**	**-36.11**	**0.1**
MPI ECHAM5	-11.21	10	-10.81	12	-1.48	73
NCAR CCSM3	+1.52	15	-0.56	9	**-11.65**	**0.1**
NCAR PCM1	+6.35	38	+4.88	30	+6.44	39

Table 3. Trends 2000–2100 in the number of days when precipitation exceeds 3 mm (top), 15 mm (middle), and 25 mm (bottom) over the Shasta, Sacramento, and Los Angeles regions from SRES A2 simulations for CNRM, GFDL, and PCM GCMs, from grid points nearest these locations. Significance determined from Monte Carlo exercise generating distribution of 1000 possible historical trends. Values that are significant at the 95% confidence level are highlighted with bold type.

Days when precipitation is > 3 mm

	Shasta		**Sacramento**		**Los Angeles**	
Model	2001 – 2100 trend	Rank (%)	2001 – 2100 trend	Rank (%)	2001 – 2100 trend	Rank (%)
CNRM CM3	**-30.37**	**0.1**	**-34.20**	**0.1**	**-9.10**	**0.1**
GFDL CM2.1	**-28.16**	**0.1**	**-23.42**	**0.1**	**-13.54**	**0.1**
NCAR PCM1	**-11.10**	**0.3**	**-12.98**	**0.1**	-5.56	7

Days when precipitation is > 15 mm

	Shasta		**Sacramento**		**Los Angeles**	
Model	2001 – 2100 trend	Rank (%)	2001 – 2100 trend	Rank (%)	2001 – 2100 trend	Rank (%)
CNRM CM3	**+2.85**	**96**	**-2.66**	**1**	**-1.12**	**3**
GFDL CM2.1	**-2.59**	**7**	**-6.04**	**1**	-0.86	29
NCAR PCM1	-0.17	58	+1.53	83	-1.00	16

Days when precipitation is > 25 mm

	Shasta		**Sacramento**		**Los Angeles**	
Model	2001 – 2100 trend	Rank (%)	2001 – 2100 trend	Rank (%)	2001 – 2100 trend	Rank (%)
CNRM CM3	**+1.04**	**99**	-0.50	17	-0.28	6
GFDL CM2.1	-0.57	23	-1.47	17	+0.09	58
NCAR PCM1	+0.60	94	**+0.91**	**95**	+0.43	70

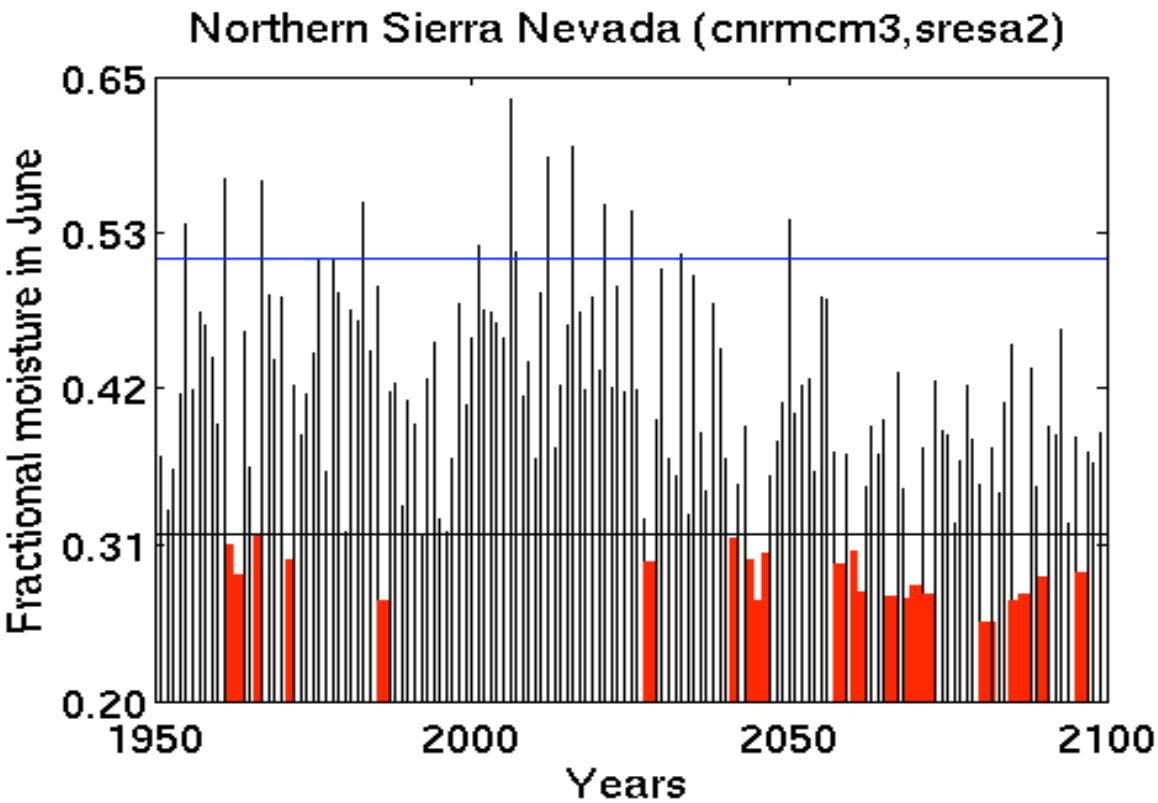

Soil Moisture (June) CNRM A2

Figure 12. June soil moisture from the Variable Infiltration Capacity (VIC) hydrological model driven by the CNRM A2 simulation downscaled using the Constructed Analogues method. Years with soil moisture being less than historical 10th percentile level are shown in red. The 90th percentile and 10th percentile June soil moisture levels are indicated by blue and black horizontal lines, respectively.

The trend toward drier conditions in California in some of these models is a response to changes in the atmospheric circulation along the eastern North Pacific and western United States margin. Although there does not appear to be much change in the wintertime (November through March) central North Pacific Aleutian low complex (Table 4), changes toward fewer storms do appear farther east along the coast of Northern California and Oregon. Regional winter season atmospheric circulation changes consistent with these changes can be seen in Figure 13 and Table 5, showing a tendency for winter (December through February) and spring (March through May) sea level pressure, in the area offshore centered at 40°N, 130°W that is most strongly linked to precipitation in the central and northern part of the state, previously named the California sea level pressure pattern (Cayan and Peterson 1989).

Table 4. North Pacific sea level pressure index (after Trenberth and Hurrell 1995), formed from average of November through March sea level pressure, 30N–65N, 160E–140W. Units are in hectopascals (hPa).

NDJFM			CNRM CM3	GFDL CM2.1	MIROC3.2 (med res)	MPI ECHAM5	NCAR CCSM3	NCAR PCM1
20C3M	1961–1990	mean	1012.57	1009.61	1006.97	1010.72	1006.74	1011.58
		sigma	2.44	3.30	2.14	2.82	3.08	3.11
SRESA2 (change from historical)	2005–2034		-0.28	-1.42	1.06	-0.45	-0.96	0.42
	2035–2064		0.97	-0.26	1.39	-0.56	-0.56	-0.27
	2070–2099		0.78	-0.83	2.62	-1,95	-0.30	-0.97
SRESB1 (change from historical)	2005–2034		0.46	-0.76	0.33	-0.54	-1.06	0.18
	2035–2064		-0.97	-1.55	0.70	-0.45	-0.62	-0.31
	2070–2099		0.17	-0.48	-0.19	-1.28	-0.99	-1.46

Consistent with the overall tendency toward somewhat drier conditions, the occurrence of significant storms, as indicated by the number of days per year when sea level pressure in the neighborhood of the San Francisco region equals or falls below 1005 millibar (mb) declines, at least marginally, in three of the models (Figure 14). Shown in Table 6, the decline in storms is stronger in the A2 simulations, in which all three simulations exhibit a decreasing trend over the 2000–2099 period that are less than the tenth percentile, according to a Monte Carlo exercise where a series of annual storm counts was randomly shuffled 1000 times to produce a distribution of 1000 such trends. The negative trends found in the San Francisco region are reinforced by the occurrence of equally or even more significant negative trends in this storm count measure in the Crescent City region. Interestingly, the storm count results are not so consistent at the La Jolla region, where only one of the six simulations reaches the 5 percentile threshold. In Figure 14, the observed occurrence of this storm measure near San Francisco from NCAR/NCEP Reanalysis is shown for comparison. In addition, the occurrence of high daily precipitation events, as indicated by daily precipitation of 25 millimeters (mm) or more, varies from year to year, but generally remains about the same level in the projected 2000–2100 climate as it was during the simulated historical period from each of the six models (Figure 15). Not surprisingly, the number of storms (using the 1005 mb threshold index) is positively correlated with the number of heavy precipitation events and also with the annual total precipitation, although these correlations are only modest (about 0.3 level). The continued occurrence of significant storms within the model simulations would suggest that future decades would continue to be occasionally affected by floods in the California region (Neiman et al. 2008).

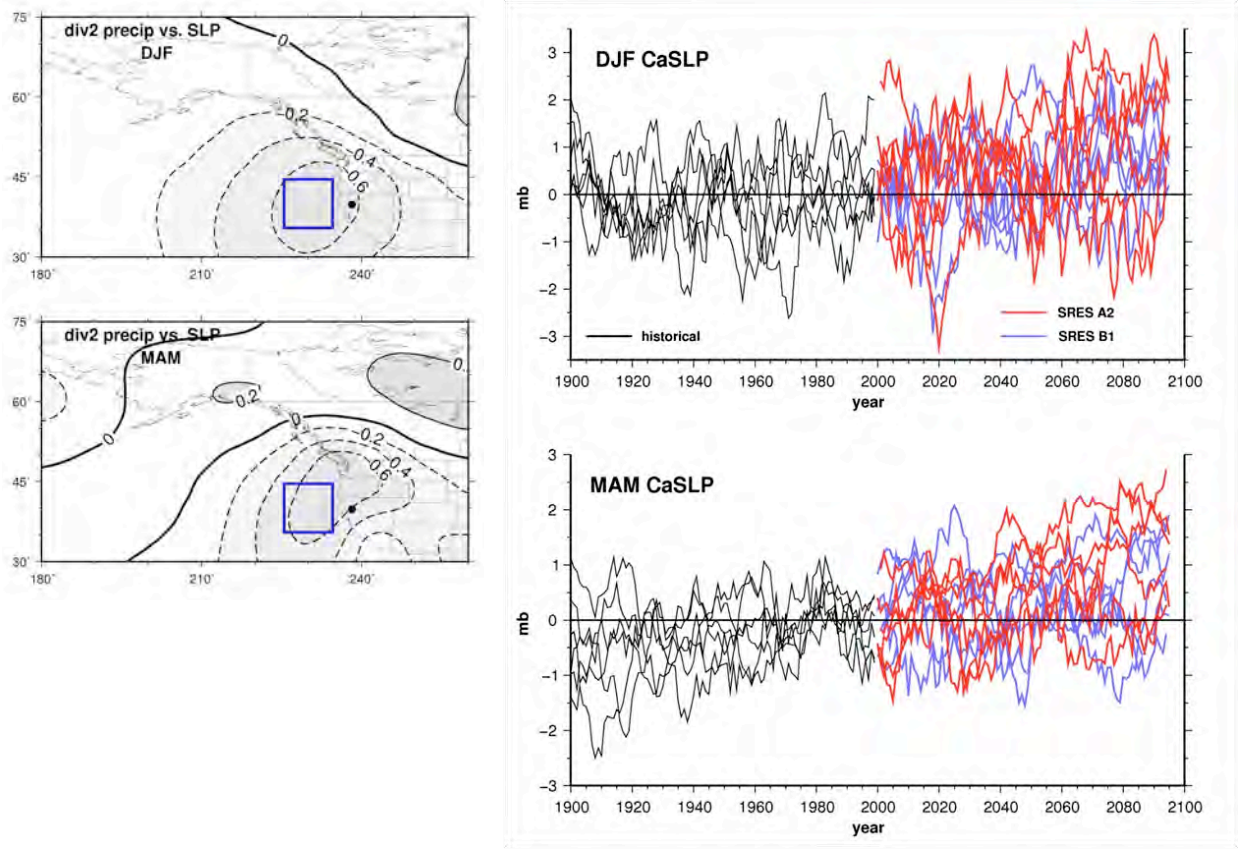

Figure 13. Simulated variability, in California sea level pressure index (CaSLP) (Cayan and Peterson 1989) for winter (upper) and spring (lower), shown in two right-hand side plots of 6 GCMs for 203CM historical simulations (black) and for B1 (blue) and A2 (red) emission scenario simulations. Maps on the left side show correlations of historical observed precipitation with NCEP Reanalysis sea level pressure, as indicated by contour lines, along with delineation of the 35-40°N, 125-135°W CaSLP "box."

Table 5. California sea level pressure index, (after Cayan and Peterson 1989) formed from average of sea level pressure centered at 40N, 130W. Units are hPa.

SON			CNRM CM3	GFDL CM2.1	MIROC3.2 (med res)	MPI ECHAM5	NCAR CCSM3	NCAR PCM1
20C3M	1961–1990	mean	1021.90	1019.70	1019.97	1020.77	1021.60	1021.35
		sigma	0.89	1.55	1.60	1.50	1.56	1.36
SRESA2 (change from historical)	2005–2034		0.00	-0.06	0.27	0.21	0.40	0.40
	2035–2064		0.27	0.66	0.16	0.18	0.75	0.17
	2070–2099		-0.12	0.21	-0.50	0.32	0.15	0.44
SRESB1 (change from historical)	2005–2034		-0.03	0.23	-0.26	0.45	0.36	0.50
	2035–2064		0.16	0.07	-0.44	0.25	0.29	0.27
	2070–2099		-0.28	0.13	-0.56	-0.32	-0.06	0.51

DJF			CNRM CM3	GFDL CM2.1	MIROC3.2 (med res)	MPI ECHAM5	NCAR CCSM3	NCAR PCM1
20C3M	1961–1990	mean	1020.69	1017.68	1019.59	1017.98	1019.53	1021.17
		sigma	2.66	3.49	2.49	3.03	2.58	4.20
SRESA2 (change from historical)	2005–2034		-1.30	-0.08	0.68	0.51	0.26	0.67
	2035–2064		1.41	0.11	1.35	0.27	0.43	0.35
	2070–2099		1.82	1.94	2.54	-0.25	1.01	-0.19
SRESB1 (change from historical)	2005–2034		0.23	-0.35	0.64	0.25	0.97	-0.93
	2035–2064		-0.50	0.06	1.59	0.00	0.31	0.59
	2070–2099		1.56	1.24	0.82	0.87	0.06	0.21

MAM			CNRM CM3	GFDL CM2.1	MIROC3.2 (med res)	MPI ECHAM5	NCAR CCSM3	NCAR PCM1
20C3M	1961–1990	mean	1021.86	1019.59	1019.50	1020.74	1021.89	1023.50
		sigma	1.39	2.83	1.90	1.36	1.62	2.67
SRESA2 (change from historical)	2005–2034		0.51	-0,15	0.25	0.11	0.19	-0.32
	2035–2064		1.51	0.61	1.03	-0.17	0.63	0.06
	2070–2099		2.28	1.70	1.44	0.12	1.00	-0.12
SRESB1 (change from historical)	2005–2034		0.53	1.25	0.64	-0.86	-0.29	0.28
	2035–2064		0.95	0.15	0.42	-0.38	0.16	-0.16
	2070–2099		1.58	0.99	1.04	-0.00	-0.00	-0.38

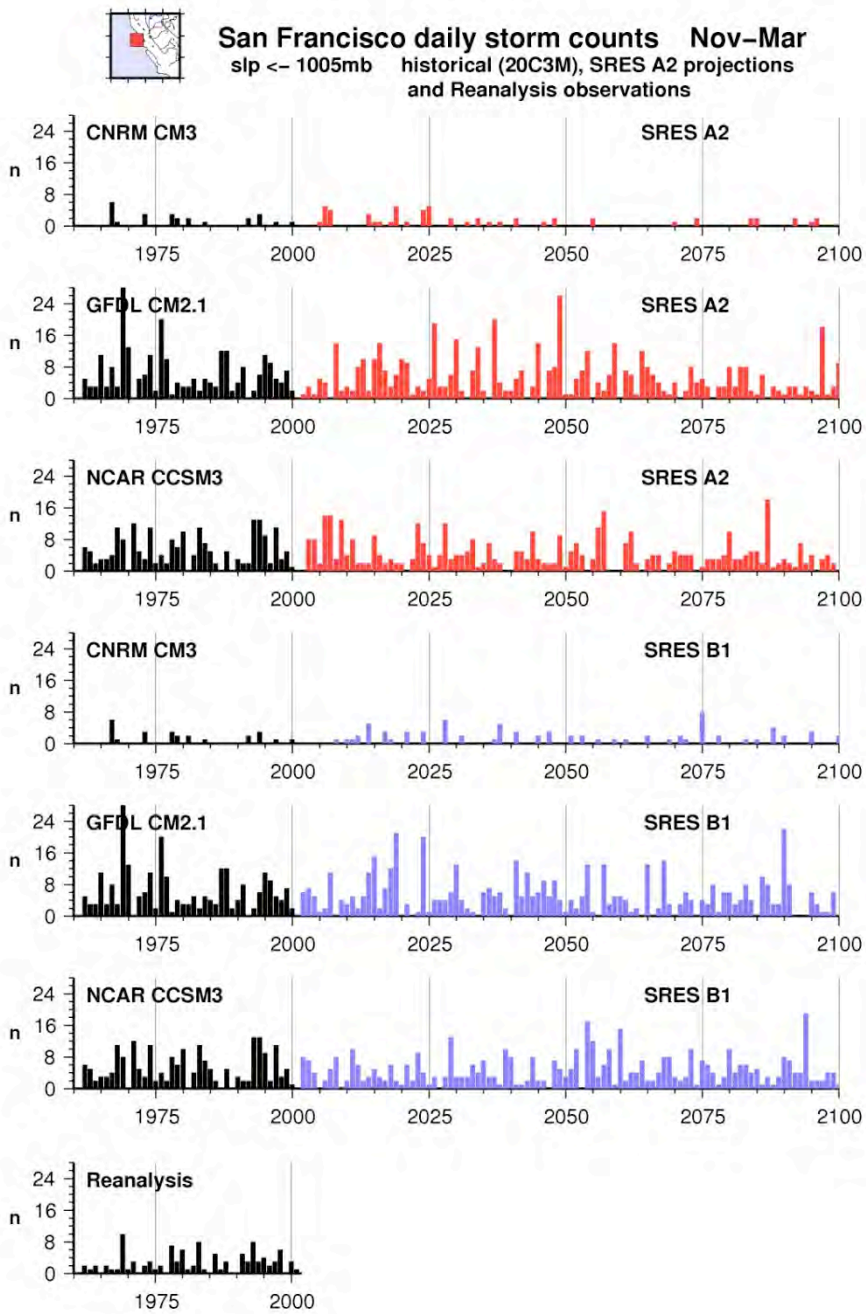

Figure 14. Number of "storms" per year as indicated by days when average daily sea level pressure (SLP) is 1005 mb or less for historical (1950–2000) (black) and projected (2001–2100) periods of the three GCMs for the B1 (below; blue) and A2 (above; red) emissions scenarios. SLP is taken directly from GCMs for the grid point nearest San Francisco.

Table 6. Trends in number of storms in the neighborhood of three regions: Crescent City, San Francisco, and La Jolla. *Storms* are defined as days having mean daily sea level pressure (SLP) less than 1005 mb in the neighborhood of Crescent City, San Francisco, or Shasta from the GCM (CNRM, GFDL, or CCSM). Percentile level of trend is indicated, as evaluated using a Monte Carlo sampling exercise. Values reaching the 90% level of significance are shown in boldface.

	Model	Scenario	Trend 2098/99 minus 2000/01	Percentile, from Monte Carlo Run
Crescent City	CNRM CM3	SRES A2	**-4.99**	**1**
	GFDL CM2.1	SRES A2	**-2.59**	**7**
	NCAR CCSM3	SRES A2	**-2.31**	**8**
	CNRM CM3	SRES B1	**-4.69**	**0.6**
	GFDL CM2.1	SRES B1	**-2.88**	**7**
	NCAR CCSM3	SRES B1	+0.57	73
San Francisco	CNRM CM3	SRES A2	**-1.01**	**0.3**
	GFDL CM2.1	SRES A2	**-2.16**	**8**
	NCAR CCSM3	SRES A2	**-2.47**	**2**
	CNRM CM3	SRES B1	-0.12	33
	GFDL CM2.1	SRES B1	**-2.00**	**9**
	NCAR CCSM3	SRES B1	+0.79	76
La Jolla	CNRM CM3	SRES A2	+0.08	78
	GFDL CM2.1	SRES A2	-0.83	13
	NCAR CCSM3	SRES A2	**-1.20**	**0.2**
	CNRM CM3	SRES B1	**+0.14**	**91**
	GFDL CM2.1	SRES B1	+0.83	87
	NCAR CCSM3	SRES B1	-0.17	35

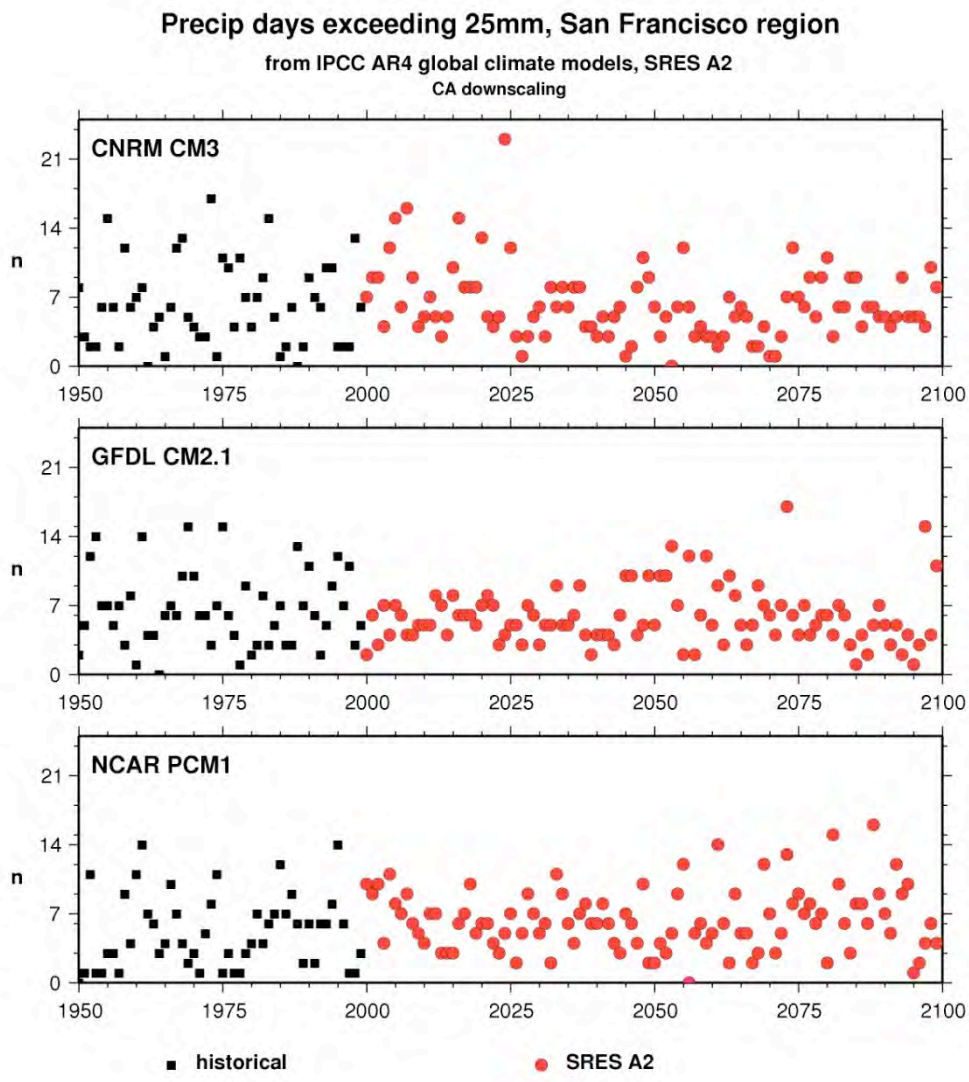

Figure 15. Number of days per year when precipitation at San Francisco equals or exceeds 25 mm. From constructed analogues downscaling of CNRM CM3, GFDL CM2.1, and NCAR PCM1 GCMs; result from BCSD downscaling (not shown) is very similar. Historical period and A2 2000–2100 projection indicated by black and red symbols, respectively. Precipitation is taken from BCSD downscaling.

7.0 El Niño/Southern Oscillation

Historically, El Niño/Southern Oscillation (ENSO) has been an important influence on weather conditions in California. The reliability of linear correlations between ENSO and precipitation is strongest in Southern California and diminishes northward. Each of the climate models contain ENSO within their historical simulations (Figure 16). Although there is no evidence for an increase in the frequency or the intensity of ENSO, each of the simulations exhibits continued ENSO activity within the twenty-first century. As displayed by observations (Redmond and Koch 1991; Gershunov et al. 2000; Cayan et al. 1999), and also during the historical GCM

simulations, there is a modest tendency for the Southern California region to experience higher than normal precipitation during El Niño winters and lower than normal precipitation during La Niña winters. To a limited degree, this pattern is also found during the climate change projections.

8.0 Sea Level Rise

Over the past several decades, sea level measured at tide gages along the California coast has risen at a rate of about 17–20 centimeters (cm) per century, a rate that is nearly the same as that from global sea level rise estimates (Church and White 2006). A paper authored by Rahmstorf (2007) demonstrated that over the last century observed global sea level rise can be linked to global mean surface air temperature. This provides a methodology to estimate global sea level using the surface air temperature projected by the global climate model simulations, and it leads to larger rates of sea level rise than those produced by other recent estimates (Cayan et al. 2008). The present estimates include those of Rahmstorf's method, assuming that sea level rise along the Southern California coast will be the same as the global estimates. Also, the projections here include a second set of estimates that are a modification of Rahmstorf's method that attempts to account for the global growth of dams and reservoirs, which have artificially changed surface runoff into the oceans (Chao et al. 2008), in addition to the effects of climate change. Using the global surface air temperature from the GCMs included in this assessment, the resulting estimates in Figures 17 and 18 indicate that potential sea level rise over the next century will increase over its historical rate by a considerable amount. Each model has a different rendition of global surface air temperature within the historical period within its "20C3M" historical simulation,[1] so that simulated historical sea levels vary between models. But in the experiments run here, the sea level estimates were adjusted so that for year 2000 their value was constrained to the same, zero value—this allows for comparison across the simulations of the amount of projected sea level rise over the twenty-first century. By 2050, sea level rise, relative to the 2000 level, ranges from 30 cm to 45 cm. As sea level rises, there will be an increased rate of extreme high sea level events (Figure 19 and Table 7), which occur during high tides, often when accompanied by winter storms and sometimes exacerbated by El Niño occurrences (Cayan et al. 2008c). Importantly, as decades proceed, these simulations also contain an increasing tendency for heightened sea level events to persist for more hours, which would seem to imply a greater threat of coastal erosion and other damage. Virtually all of the increase in frequency and magnitude of sea level exceedances can be ascribed to the underlying secular increase in mean sea level. The increase in exceedances cannot be attributed to a change in weather activity, as demonstrated by running the sea level model with weather-forcing only, as summarized in Table 8. This steady behavior in weather is consistent with the relative lack of major changes in the Aleutian Low system (not shown).

[1] For example, see www.ccsm.ucar.edu/working_groups/Change/CCSM3_IPCC_AR4/20C3M.html.

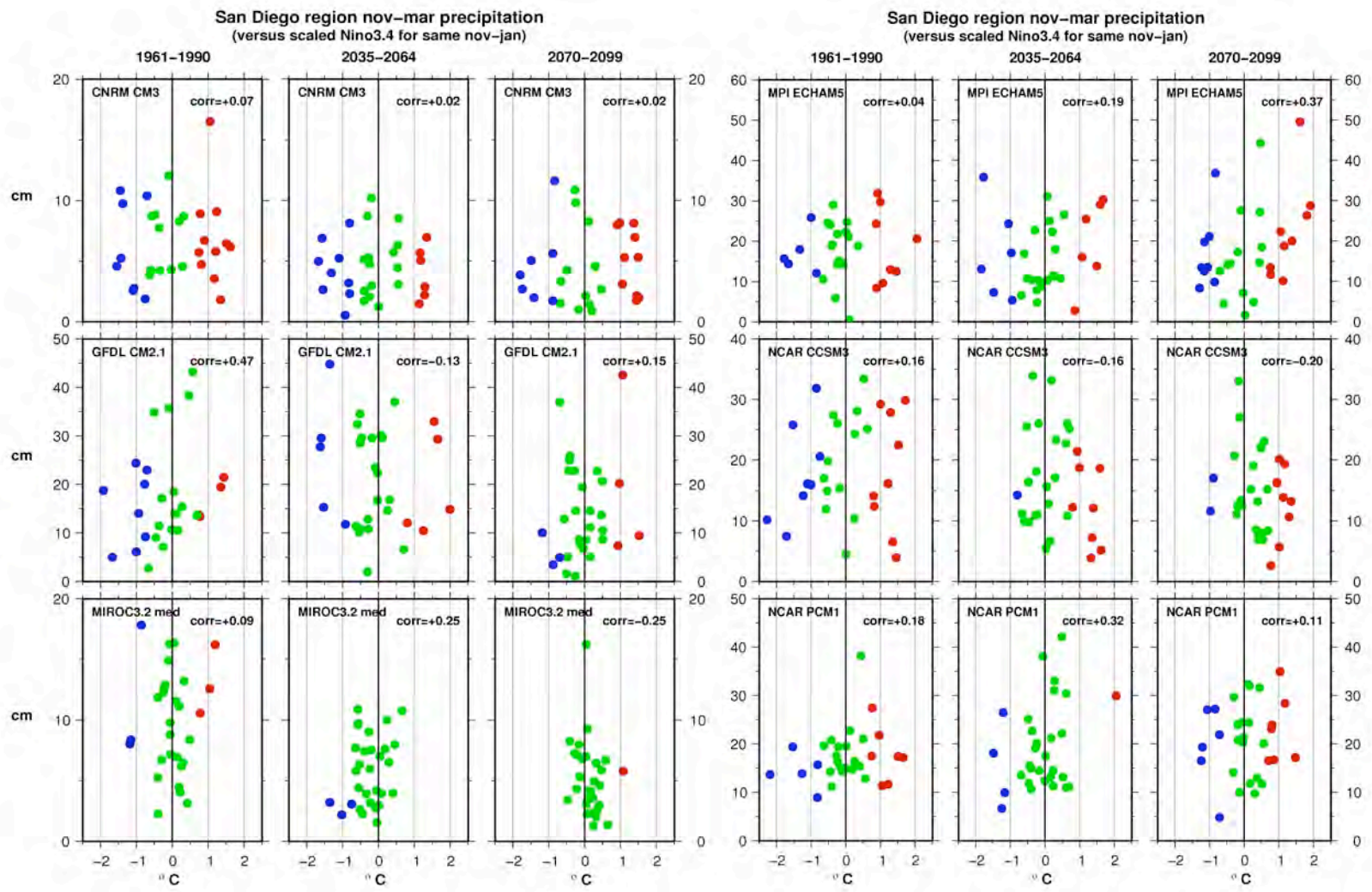

Figure 16. Association of precipitation in San Diego region to ENSO, as indicated by the El Niño 3.4 sea surface temperature (SST) index, which is the area average sea surface temperature departure from the historical average in the central equatorial Pacific Ocean. Projected Niño 3.4 SST series have been adjusted by removing the linear trend to better discern interannual fluctuations. Precipitation values during cool, neutral, and warm Niño 3.4 SST

years indicated by blue, green, and red dots respectively. San Diego region precipitation extracted directly from each of the GCMs, from the grid point nearest to San Diego.

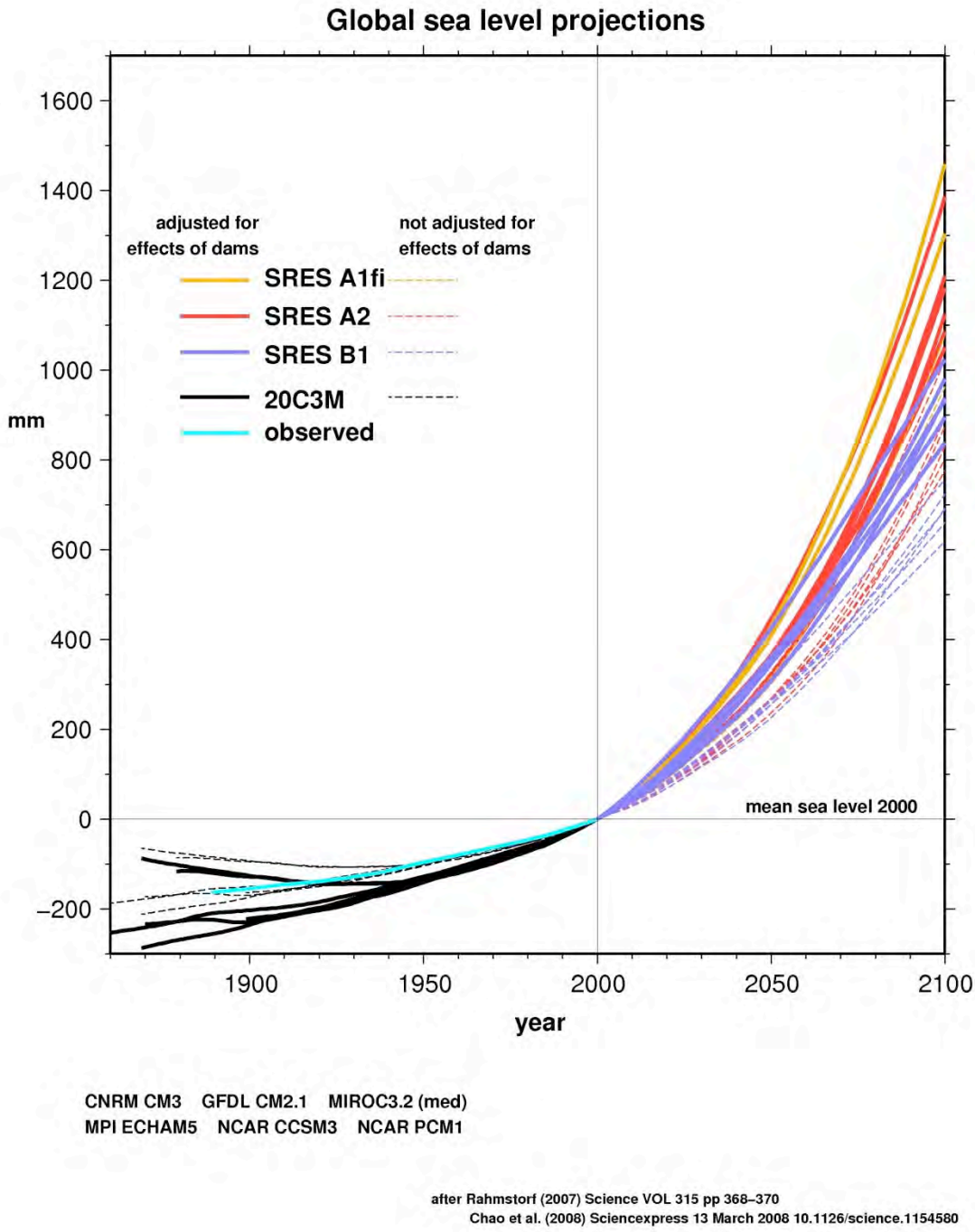

Figure 17. Projected global sea level using the Rahmstorf (2007) scheme from each of the six models (set to zero at 2000). Climate change simulations for the SRES A1fi, A2 and B1 emission scenarios are shown for both the original Rahmstorf (dashed curves) and a version adjusted for the affect of reservoirs and dams (solid). Historical (black) and projected B1 simulations (blue), A2 simulations (red), A1fi (gold) are shown along with observed global sea level (aqua).

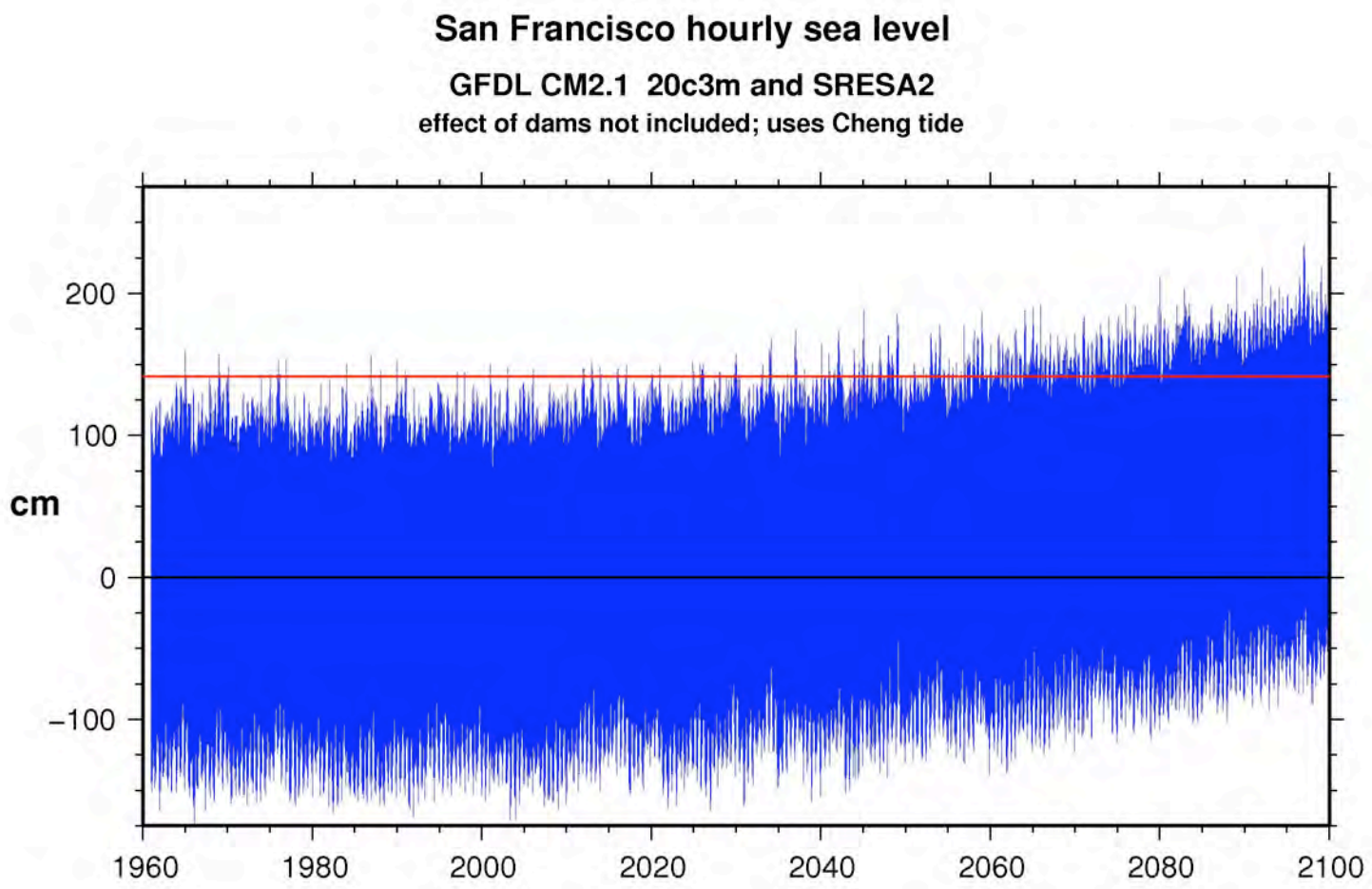

Figure 18. Hourly sea level simulated for San Francisco (Fort Point) location, using secular change estimated using the Rahmstorf (2007) scheme. Hourly sea level model from Cayan et al. 2008c includes this secular rise and superimposes predicted astronomical tides, barometric pressures winds, and ENSO from GFDL A2 simulation. Sea level values are referenced to the long-term mean historical average.

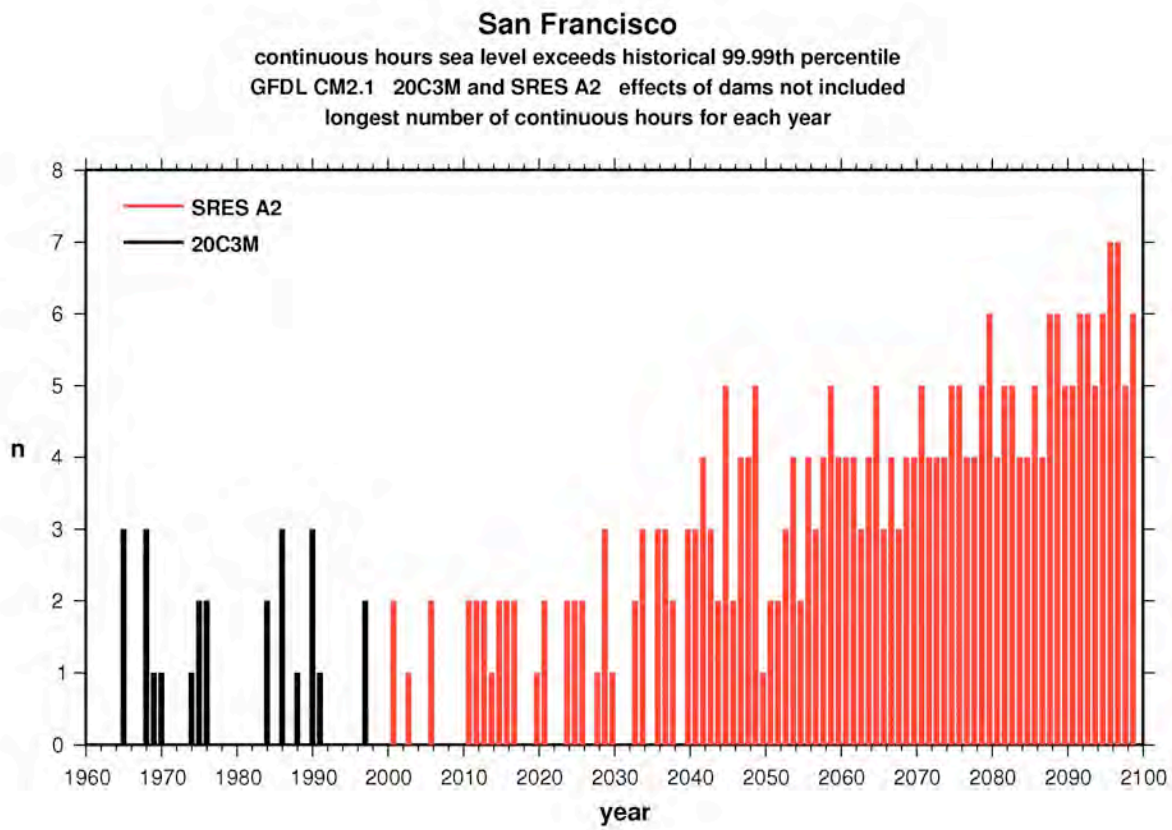

Figure 19. Maximum duration (hours) that San Francisco sea level, as depicted in Figure 18, exceeds the 99.99th percentile level (140 cm above mean sea level), as modeled from the GFDL historical (20C3M) simulation (black) and the GFDL climate change (SRESA2) simulation (red) using the Rahmstorf sea level scheme without adjustment for effect of dams

Table 7. Hourly Sea Level Exceedances, San Francisco. Number of hours and percent of total hours sea level exceeds the 99.99th historical (1960–1978) percentile for each 30 year period. The 99.99th historical percentile is 141 cm.

Model	Scenario	2005–2034	2035–2064	2070–2099
CNRM CM3	SRESB1	64 (0.02%)	810 (0.31%)	10428 (3.97%)
	SRESA2	32 (0.01%)	627 (0.24%)	19225 (7.32%)
GFDL CM2.1	SRESB1	161 (0.06%)	1112 (0.42%)	9304 (3.54%)
	SRESA2	108 (0.04%)	1206 (0.46%)	15447 (5.88%)
NCAR CCSM3	SRESB1	217 (0.08%)	2108 (0.80%)	16768 (6.38%)
	SRESA2	171 (0.07%)	2480 (0.94%)	34736 (13.22%)

(2008 sea level model; Rahmstorf scheme, no adjustment for dams)

Table 8. Standard deviation of hourly sea level (cm) from the weather component of the sea level model

		La Jolla			San Francisco			Crescent City		
		CNRM CM3	GFDL CM2.1	NCAR CCSM3	CNRM CM3	GFDL CM2.1	NCAR CCSM3	CNRM CM3	GFDL CM2.1	NCAR CCSM3
20C3M	1961–1990	2.93	4.47	4.11	5.56	8.41	8.90	9.15	11.35	12.19
SRESA2	2005–2034	3.00	4.53	4.22	5.87	8.03	9.04	9.74	11.18	12.53
	2035–2064	2.83	4.58	3.96	5.33	8.41	8.88	9.22	11.61	12.33
	2070–2099	2.92	4.35	3.90	5.71	7.77	8.65	9.88	10.90	11.98
SRESB1	1961–1990	3.02	4.42	4.07	5.82	8.36	8.83	9.51	11.36	12.23
	2035–2064	2.88	4.42	4.06	5.62	8.26	9.06	9.38	11.21	12.24
	2070–2099	2.92	4.38	4.09	5.61	7.95	9.01	9.37	10.86	12.24

9.0 North Pacific Wind Waves along the California Coast

Wind wave modeling was conducted over the North Pacific, with emphasis on the waves that impinge upon the California coast. The model used is the Wavewatch III v1.18 wave model (Tolman 1998), configured at a resolution of 1.0 x 1.5 degrees latitude / longitude using 20 frequency bands covering the range of periods 27.2 to 4.4 seconds and using a directional resolution of 5 degrees. The spatial domain covers the entire North Pacific Ocean from 20N to the coasts of Asia, the Aleutian Islands, and North America. The ocean is treated as flat bottomed, 1000 meters deep (i.e., there is no refraction); there are no currents or sea ice included.

Six simulations were conducted:

- RA – NCEP Reanalysis nominal "10 meter (m) mean sea level (MSL)" winds, 1948–1999, native resolution about 1.8 degrees latitude / longitude.
- CCSM-20C – NCAR CCSM using the IPCC SRES twentieth-century emissions scenario, native resolution about 1.4 degrees latitude and longitude. Time covered is 1941–1999; winds are from the lowest model level at approximately 60 m MSL.
- CCSM-A1B – NCAR CCSM using the IPCC SRES A1B emissions scenario, native resolution about 1.4 degrees latitude and longitude. Time covered is 2000–2099; winds are from the lowest model level at approximately 60 m MSL.
- CCSM-A2 – NCAR CCSM using the IPCC SRES A2 emissions scenario, native resolution about 1.4 degrees latitude and longitude. Time covered is 2000–2099; winds are from the lowest model level at approximately 60 m MSL.
- CNRM-20C – CNRM GCM using the IPCC SRES twentieth-century emissions scenario, native resolution about 1.8 degrees latitude and longitude. Time covered is 1970–1999; winds are nominally from 10 m MSL.
- CNRM-A2 – CNRM GCM using the IPCC SRES A2 century emissions scenario, native resolution about 1.8 degrees latitude and longitude. Time covered is 2000–2099; winds are nominally from 10 m MSL.

All simulations used the available six-hourly wind data. The wave model used a nominal one-hour time step, with a sub-step adaptive time step depending on the generation characteristics.

Tuning (spatially and temporally fixed) was conducted to bring the wave climatologies from the CCSM-20C and CNRM-20C simulations into approximate congruence with the NCEP Reanalysis simulation. The latter was tuned in earlier simulations using the NCEP Reanalysis winds to give good agreement for larger wave events at buoys in the eastern North Pacific. There is some low bias for waves driven by near-coastal winds along the California coast. This is due primarily to wind speed bias in the NCEP Reanalysis wind data near the coast, a result of the rather coarse atmospheric general circulation model resolution and the importance of coastal effects in the wind climatology of this region. This bias has very little effect on the results here. Comparison of the NCEP Reanalysis results with buoy data for larger wave events is quite good; with correlations for many years of three-hourly data in winter of about 0.9 (Graham 2005).

The North Pacific near-surface wind climatology of the CCSM model is quite good (not shown). The tuning used a relatively simple boundary layer model, similar to Liu et al. 1979, to adjust the raw CCSM winds to near-surface winds. After a series of trial simulations the tuning resulted in a wave climatology for the California coast that is essentially indistinguishable from the NCEP Reanalysis results for the period 1978–1999. The CNRM near-surface wind climatology over the North Pacific is less realistic than for the CCSM model, but after several trial simulations satisfactory overall winter wave climatology was obtained with a modest low bias (about 0.4 m) along the California coast.

The CCSM-A1B, CCSM-A2, and CNRM-A2 simulations were examined for 2000–2001 to 2098–2099. The annual November–March (NDJFM) fiftieth and ninety-ninth percentile climatologies

for approximately the year 2000 are shown (the 2001–2099 climatology less half the trend over that period) along with the trends in NDJFM fiftieth and ninety-ninth percentile significant wave heights (Hs50 and Hs99, respectively) expressed as meters per century and as percentages of the climatologies described above. The CCSM trends are statistically significant and negative for Hs50 south a line roughly following the typical storm track from about 35N along the coast of Asia to near 60N and the North American coastline. Near the coast of California these trends are typically 5%–10% (declines) of the year 2000 climatology. For Hs99 the trends are generally not statistically significant except off the coast of Asia. The lack of significance is probably due to the "noisier" nature of ninety-ninth percentile statistics and would likely appear qualitatively much like the Hs50 results if the many ensemble simulations were performed.

For the CCSM-A2 simulation the trends are significant for both Hs50 and Hs99 and follow the same pattern as the CCSM-A1B fiftieth percentile results and show significant negative trends amounting to 5%–10% (declines) of the year 2000 climatology for Hs50 with slightly smaller magnitudes for Hs99.

For the CNRM-A2 results the pattern of trends is similar to those described for the CCSM-driven results with mostly negative trends in the southern part of the domain and mostly positive trend farther north and the largest negative trends off the coast of Japan. Trends along the California coast are only marginally statistically significant and are about 3%–5% declines for Hs50 and 5%–10% declines for Hs99.

Overall, the model results are quite satisfactory in providing information about likely scenarios of winter wave height changes along the California coast. The pattern of negative trends to the south with a tendency toward positive trends to the north reflects a decrease of winter storm wind forcing. This is produced as the mean cyclone track tends to move north as the climate warms, a robust feature of greenhouse climate change simulations reflecting in part the warming of the higher land masses and oceans (and declining sea ice coverage) and the expansion of the subtropical high pressure regions. The lower waves of California is thought to be largely due to this northward migration of the storm track (this shift is clear, but rather small—on the order of 1 degree (latitude)—and may also reflect some decrease in cyclone intensity. The consistency of the wave modeling results is heartening with the suggestion of slight negative trends in wave heights, with larger negative and more significant trends with higher greenhouse gas concentrations. It should be noted that the trends along the California coast, shown in Figure 20 for the Northern California coast and in Figure 21 for Point Conception, are generally marginally significant. The simulations clearly suggest that interannual (not shown) and inter-decadal fluctuations in larger wave episodes (as indexed by Hs99) will continue to dominate wave climate impacts as they have in the past. A final point is that these results indicate that the positive trends in eastern North Pacific winter wave heights noted over the latter half of the twentieth-century are very likely due to natural climate variability rather than anthropogenic warming.

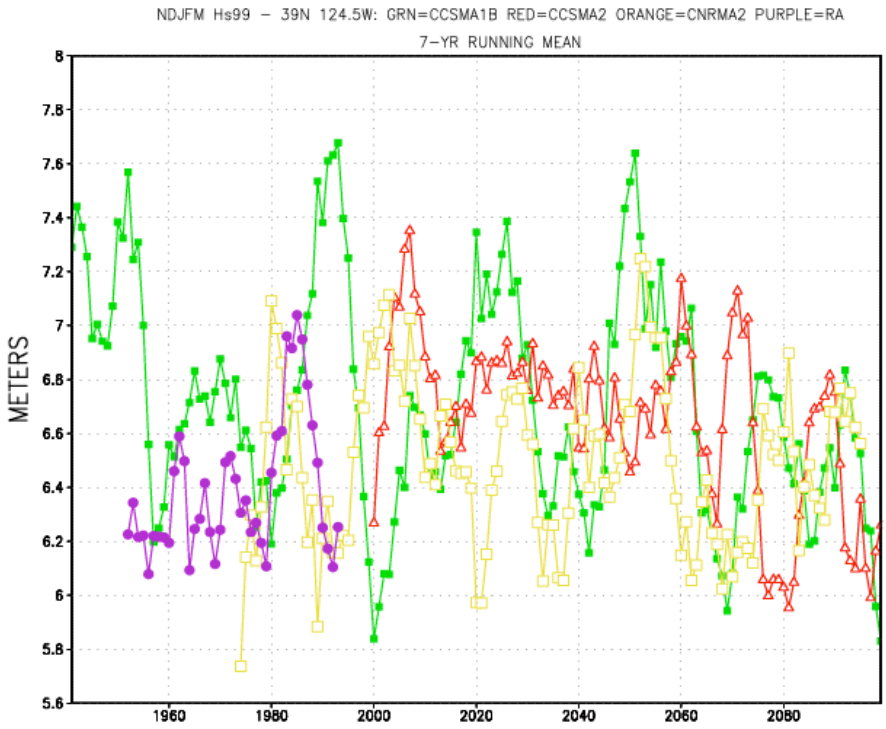

Figure 20. The 99th percentile significant wave heights (Hs99), November through March for Reanalysis (purple), and CCSM A1 (green), CCSM A2 (red), and CNRM A2 climate simulations for Northern California coast offshore from San Francisco. Series have been smoothed with a 7-year running mean.

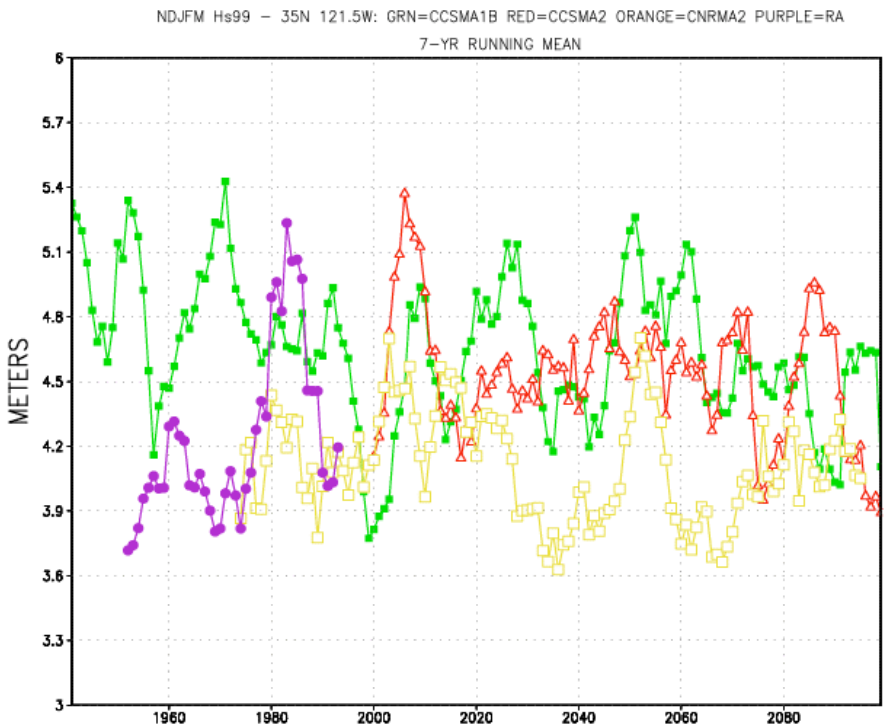

Figure 21. The 99th percentile significant wave heights (Hs99), November through March for Reanalysis (purple), and CCSM A1 (green), CCSM A2 (red), and CNRM A2 climate simulations for location offshore from Point Conception. Series have been smoothed with a 7-year running mean.

10.0 Shore Zone Wave Runup Variability

Rising sea level in response to climate change allows more wave energy to reach farther shoreward, increasing the potential for greater coastal impacts. Mean sea level is the base level on which shorter duration fluctuations (such as El Niño-related increases, tides, storm surge, and waves) are superimposed. Coincident occurrence of extremes in these short-term fluctuations results in the greatest coastal impacts. Rising sea level augments extreme sea level fluctuations, causing increased coastal erosion potential from wave activity. This is investigated using a model of the runup of waves onto an idealized Central California beach.

Beach erosion, exacerbated by rising sea levels, can potentially have a serious impact on the economy of Southern California. Depending upon the rate that sea level rises during the twenty-first century, many beaches will shrink in width, and some beaches may disappear entirely.

Waves provide nearly all the energy that drives physical processes along coasts, and the occurrence of high waves coincident with sea level and tidal extremes is of critical importance.

Projections of wave height and directional wave spectral estimates offshore California were generated for winter months (November–March, when the highest waves occur along the California coast) over the twenty-first century using the WAVEWATCH III (WWIII; Tolman 2002) wave model with forcing by NCAR CCSM3 global climate model winds for the high greenhouse gas A2 emissions scenario.

Previous work has shown that winds from this GCM generate waves that compare reasonably well statistically with coincident observations from buoys along the coast (Graham and Diaz 2001). Wave heights decrease from north-to-south (Table 9), reflecting the dominant pattern observed in historical NOAA buoy data (Bromirski et al. 2005). The winter ninety-eighth percentile significant wave height (*Hs*, the average of the highest one-third of the waves) at three locations that span the California coast have downward trends (Figure 22), likely associated with either decreased model winds or a northward shift in storm track in response to climate change. This projected tendency for decreased extreme waves could partially compensate for the expected significant rise in sea level (Figure 17), somewhat reducing the projected coastal erosion potential. It should be noted that these model wave heights result from model winds from one realization of a single GCM, and it is uncertain how closely these projections will match future observations.

The largest or fastest beach and shoreline changes can generally be associated with the maximum wave runup—the height of discrete water-level maxima at the shore. To investigate potential changes due to the combination of wave variability and sea level rise, runup projections using the directional wave and sea level projections were determined. Because beach-face slopes vary both spatially and temporally, three low-to-moderate fixed beach slopes were selected. Runup depends on the nearshore deep-water wave height, H_0, and its associated wavelength, L_0, and the beach slope, β, as well as geology (e.g., headlands, bedrock outcrops) and exposure (local coastline configuration and bathymetry).

There is considerable uncertainty in the variability of the near-coastal wave climate and the associated erosion response of beaches to wave activity, as well as the reliability of model projections of wave and sea level extremes. Wave direction can vary significantly between storms during winters. Interannual and seasonal changes in nearshore bathymetry can greatly affect the amount of wave energy reaching the shore at specific locations. The current understanding of coastal wave processes and beach response is not sufficient to model the long-term beach evolution in response to changes in wave and sea level extremes. Furthermore, observationally based runup models incorporate empirically determined coefficients (Stockdon et al. 2006), which may have significant site dependence not accounted for. Because of these and runup model uncertainties, the empirical runup formulation of Stockdon et al. (2006, eqn. [19]) provides adequate runup estimates for projected model wave spectra and sea levels for non-specific beach configurations, and it was used to obtain the runup estimates presented here.

The non-wave instantaneous relative sea level projection represents the "still water level" (SWL), i.e., the base water level from which wave-induced runup estimates are projected shoreward. The SWL estimate at the time of each model directional wave spectrum estimate processed was obtained from the hourly sea level projections.

Wave conditions at the coast depend both on the wave conditions offshore and, critically, on their transformation as they travel over the continental shelf and into the nearshore zone. The

projected wave energy (frequency-directional wave spectra) from near-coastal deep-water sites associated with the top 10% of the model *Hs* estimates in each winter (about 120) were transformed to near-shore locations using the linear refraction model of O'Reilly (1991). This gives a sufficiently large sample size to obtain a stable estimate of extreme winter runup variability. The transformed wave spectra provide the input parameters for coastal runup modeling. The peak in the transformed wave spectrum gives the peak wave period, and its associated wavelength L_0 is used in the runup model computation.

The transformed nearshore wave spectra were used to generate wavetrains of three-hour duration having randomized phase. This wavetrain time series length was selected to ensure an adequate statistical sampling of 20 s period waves, the maximum wave period generally expected to be observed. Individual waves (successive peak-to-trough heights) within each wavetrain were ranked according to amplitude, with the ninety-eighth and fiftieth percentiles identified. These percentiles served as the wave height estimate H_0 in the runup model.

Wave heights vary in concert along the California coast. That is, when high waves are observed along the north coast, they are generally observed along most of the coast to the south, and vice versa (Bromirski et al. 2005). Wave conditions in the San Francisco region are representative of most of the California coast, so generalized runup estimates in that region are also likely representative. To assess potential trends and long-term variability, runup projections were made for directional wave spectra offshore Central California at 38°N 124.5°W, transformed to 15 m water depth at San Francisco's Ocean Beach (37.733°N 122.606°W).

Winter averages of runup give an indication of trends and long-term variability (Figure 23) using the A2 model waves for both A2 and B1 sea level projections (the sea level projections used include the future dam-construction correction factor). The greatest differences between A2 and B1 mean winter runup levels for the ninety-eighth percentile H_0 estimates occur during the latter half of the twenty-first century, dominated by the acceleration in projected sea level (Figure 17). Comparison of Figures 22 and 23 indicates, as would be expected, that high mean winter runup appears to be associated with peaks in extreme winter wave heights, although the upward trends must be dominated by rising sea level.

Because of the multiple uncertainties associated with absolute runup projections, percentage changes associated with changing wave and sea level conditions likely have the most significance. The percentage increases in runup are greatest for lower foreshore beach slopes, suggesting that these beaches will be most vulnerable under rising sea levels. Percentage increases for the fiftieth percentile wave heights (not shown) are substantially greater (~50%) than for the ninety-eighth percentile waves for all foreshore beach slopes, suggesting that moderate waves will have a greater impact on beach erosion processes under higher sea levels in the future.

An upward trend in wave energy has been observed in the eastern North Pacific during recent decades (Bromirski et al. 2005). If this pattern should continue, or at least maintain its recent climatological level, the downward trend in projections of wave model extremes will not be realized, and given the projected sea level rise, the coastal erosion potential would increase even more than in the present scenarios.

Table 9. Projected WWIII model significant wave height, *Hs*, percentile levels at Crescent City (CRE), San Francisco (SFO), and San Miguel Island (SML) over all 2000–2099 winters (November–March)

Percentile	25	50	75	90	99
CRE	1.90	2.84	4.04	5.37	8.10
SFO	1.71	2.46	3.38	4.43	6.68
SML	1.36	1.96	2.67	3.46	5.23

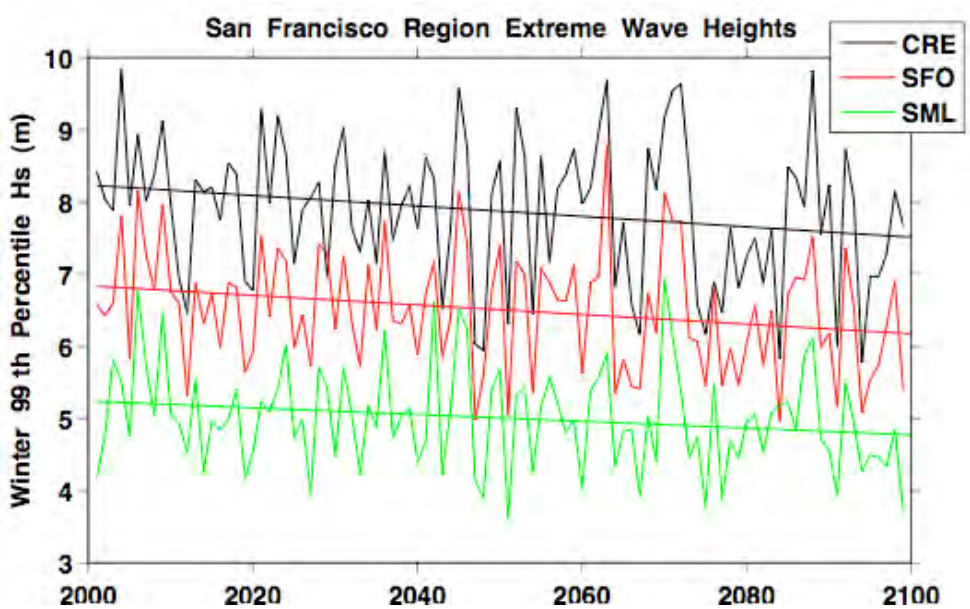

Figure 22. Winter (Nov.–Mar.) 99th percentiles of the WAVEWATCH III model significant wave height, *Hs*, projections forced by NCAR CCSM3 model winds. Offshore locations at northern California near Crescent City (CRE, 42°N 126°W; black), Central California near San Francisco (SFO, 38°N 124.5°W; red), and Southern California near San Miguel Island (SML, 34°N 121.5°W; green) are shown. Downward least squares trends steepen slightly going northward. These downward trends represent about a 9% decrease.

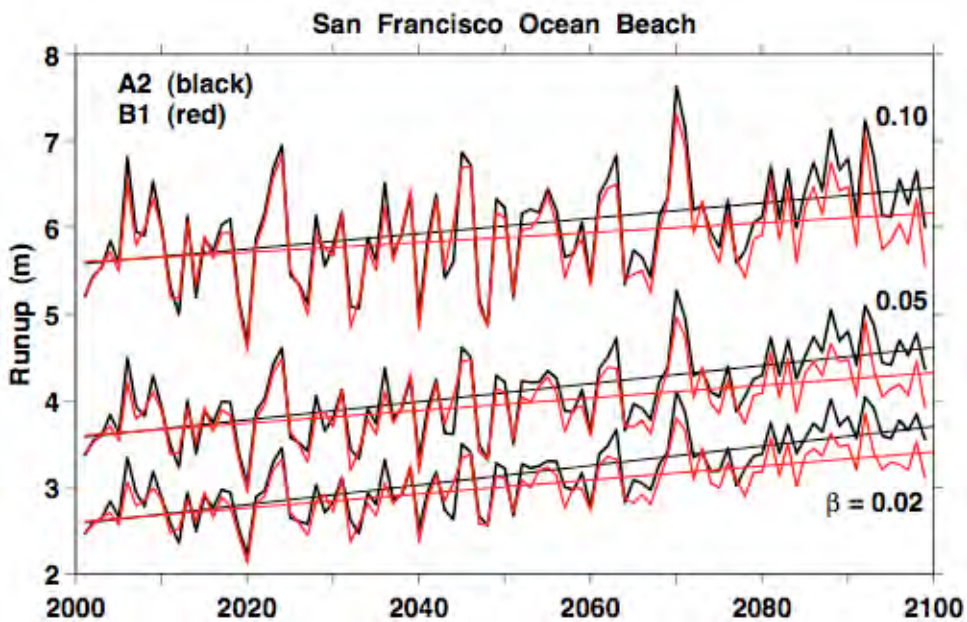

Figure 23. Projected mean winter (Nov.-Mar.) runup for the 98th percentile wave H_0 amplitudes for both low, B1 (red) and high, A2 (black) GHG emission scenario sea level projections. Low to moderate foreshore beach slopes, β, have upward trends with associated changes of 43%, 29%, and 16% for A2 and 31%, 20%, and 10% for B1 for β = 0.02, 0.05, 0.10, respectively.

11.0 Discussion

A set of simulations of possible twenty-first century climate in California were investigated. They are being used as drivers of impacts in a variety of sectors in the state, so it is important to understand the structure and changes that are contained in these simulations. The first-order surface climate variables, temperature, and precipitation—and some immediate implications for snowpacks and runoff in California—were the focus of the present study. The projections analyzed were based upon simulations by global climate models and associated statistically downscaled counterparts. Although regional models will be needed to distribute climate over the complex landscape of California, the first-order climate changes tend to derive from the large, indeed global, scale responses to increasing GHGs, even when considered at the California scale. These projections were based upon six global climate models forced by the SRES B1 and SRES A2 greenhouse gas emission scenarios. These projections are not "predictions," but are, based upon current understanding, plausible scenarios of climates that may occur in the twenty-first century.

Physical aspects of the climate scenarios in the present investigation are consistent with those described in previous studies and, in particular, those described in the previous 2005–2006 California climate scenarios assessment. This latest version reinforces, and in certain respects amplifies, the previous results, introducing climate simulations from four additional global climate models (GCMs).

Some clear results emerge from these simulations—these reiterate findings from many previous studies. Rising temperatures and rising sea levels are found in all of the projections, although the amount of change is still uncertain. The simulations also contain variability time scales from synoptic to multidecadal, but their general tendency is to rise quite steadily and rather linearly over the twenty-first century. As the differences in greenhouse gases accumulate from the higher (A2) versus the lower (B1) scenarios, the differences in warming mount, and the difference in global and regional (California) temperature also grows. From a method described by Rahmstorf (2007) using global air temperature to determine sea level rise, the simulations with higher warming result in greater rates of sea level rise. The range of sea level rise from the beginning to the end of the twenty-first century, as derived by the present analysis, range from about 0.5 meters (m) to 1.4 m, which is significantly larger than the estimates reported by a somewhat different methodology in the previous California Climate Change Scenarios study (Cayan et al. 2008). It is notable that until about the middle of the twenty-first century, different emissions scenarios do not too produce much difference in temperature, but thereafter the warming of the A2 scenario becomes increasingly distinct, and larger than that in the B1 scenario. As temperatures rise, so does sea level and so does wave runup along California beaches and the loss in spring snowpack in the Sierra Nevada. The incidence of years with very low spring snowpack and associated low soil moisture in late spring and early summer occur much more frequently. Also, as temperatures rise, there is a substantial increase in the occurrence, magnitude, and duration of certain kinds of extremes, such as heat waves and high sea level events. These short period events will have great impacts on California's natural and societal systems.

Other results from the simulations are more variable across models and across simulations using the same model, but contain some noteworthy tendencies that also have serious implications. Asymmetries in warming (warmer in summer than winter, and warmer in the interior than along the coast) that occur in some of the models would have important impacts for California's climate. The magnitude of these asymmetries can be fairly large, which underscores the importance of investigating climate changes in more detail than from simply investigating mean annual temperature and other average measures. The set of models' precipitation changes do not present the equivalent uniformity nor the relentless increases throughout the twenty-first century as do those for temperature, but there is a disquieting preponderance of simulations that become significantly drier during the twenty-first century. This drying appears to be linked to a rise in sea level pressure in the key storm track and wind wave and precipitation generating regions across the North Pacific and along Northern California and Oregon's Pacific coast. Seven of these simulations contain mid- and late-twenty-first century 30-year averages with precipitation deficits within -5% to -15% of our 1961–1990 climatology. It is useful to put these levels into historical perspective. Using the National Climatic Data Center Sacramento drainage divisional precipitation division record beginning 1895, a running tally of 30-year averages finds a high of +14.6% to a low of -2.7%, or if we change the standard climatology to a different 30-year period, a range of about -8.6% to +8.6%. Thus, the drying changes that are projected are rivaling or exceeding the largest observed multi-decadal deficits within the modern California historical experience. Should these drying trends materialize, they would present a challenge to sustaining many of California's societal structures and its ecosystems.

Consistent with the decline in precipitation described above, in some of the simulations the incidence of large coastal storms and the level of wind wave energy reaching much of the California coast decreases, at least marginally, over the twenty-first century. Thus, in addition to our future research to understand future impacts of warming, sea level rise, and drought, it is important to study event-scale process such as coastal erosion and flood events.

12.0 References

Barnett, T., R. Malone, W. Pennell, D. Stammer, A. Semtner, and W. Washington. 2004. "The effects of climate change on water resources in the west: Introduction and Overview." *Climatic Change* 62:1–11.

Barnett, T. P. et al. 2008. "Human-Induced Changes in the Hydrology of the Western United States." *Science* 319(5866): 1080–1083, DOI: 10.1126/science.1152538.

Bonfils, C., P. Duffy, B. Santer, T. Wigley, D. B. Lobell, T. J. Phillips, and C. Doutriaux. 2007. "Identification of external influences on temperatures in California." *Clim. Ch.* 87:43–55.

Bonfils C., B. D. Santer, D. W. Pierce, H. G. Hidalgo, G. Bala, T. Das, T. P. Barnett, D. R. Cayan, C. Doutriaux, A. W. Wood, A. Mirin, and T. Nozawa. 2008. "Detection and attribution of temperature changes in the mountainous western United States." *J. Climate* In press.

Brekke, L. D., M. D. Dettinger, E. P. Maurer, and M. Anderson. 2008. "Significance of model credibility in projection distributions for regional hydroclimatological impacts of climate change." *Climatic Change* 89:371–394. doi:10.1007/s10584-007-9388-3.

Bromirski, P. D., D. R. Cayan, and R. E. Flick. 2005. "Wave spectral energy variability in the Northeast Pacific." *J. Geophys. Res*. 110, C03005, doi:10.1029/2004JC002398.

Cayan, D. R., and D. H. Peterson. 1989. The influence of North Pacific atmospheric circulation on streamflow in the West. Geophys. Monograph 55: Aspects of Climate Variability in the Pacific and the Western Americas. December 1989, 375–397.

Cayan, D. R., K. T. Redmond, and L. G. Riddle. 1999. "ENSO and Hydrologic Extremes in the Western United States." *Journal of Climate* 12: 2881–2893.

Cayan, D. R., A. L. Luers, G. Franco, M. Hanemann, B. Croes, and E. Vine. 2008a. "Overview of the California climate change scenarios project." *Climatic Change* 87(Suppl 1): S1–S6, doi:10.1007/s10584-007-9352-2.

Cayan, D. R., E. P. Maurer, M. D. Dettinger, M. Tyree, and K. Hayhoe. 2008b. "Climate Change Scenarios for the California Region." *Climatic Change*, published online, 26 Jan. 2008, doi:10.1007/s10584-007-9377-6

Cayan, D. R., P. D. Bromirski, K. Hayhoe, M. Tyree, M. D. Dettinger, and R. E. Flick. 2008c. "Climate change projections of sea level extremes along the California coast." *Climatic Change* 87(Suppl 1): S57–S73, doi:10.1007/s10584-007-9376-7.

Chao, B. F., Y. H. Wu, and Y. S. Li. 2008. "Impact of Artificial Reservoir Water Impoundment on Global Sea Level." Science 320(5873): 212–214. 11 April 2008, DOI: 10.1126/science.1154580.

Church, J. A., and N. J. White. 2006. "A 20th century acceleration in global sea-level rise." *Geophys. Res. Lett.* 33. L01602, doi:10.1029/2005GL024826.

Coquard, J., P. B. Duffy, K. E. Taylor, and J. P. Iorio. 2004. "Present and future surface climate in the western USA as simulated by 15 global climate models." *Climate Dynamics* 23(5): 455.

Field, C. B., G. C. Daily, F. W. Davis, S. Gaines, P. A. Matson, J. Melack, and N. L. Miller. 1999. *Confronting Climate Change in California: Ecological Impacts on the Golden State.* Union of Concerned Scientists, Cambridge, Mass., and Ecological Society of America, Washington, D.C.

Franco, G., D. Cayan, A. Luers, M. Hanemann, and B. Croes. 2008. "Linking climate change science with policy in California." *Climatic Change* 87(Suppl 1): S7–S20, doi:10.1007/s10584-007-9359-8.

Gershunov, A., T. P. Barnett, D. R. Cayan, A. Tubbs, and L. Goddard. 2000. "Predicting ENSO Impacts on Intraseasonal Precipitation Statistics in California: The 1997–1998 Event." *J. of Hydromet*. 1(6): 201–210.

Gershunov A., and H. Douville. 2008. Extensive summer hot and cold extremes under current and possible future climatic conditions: Europe and North America. In: H. Diaz, and R. Murnane (Eds.), *Climate Extremes and Society*. Cambridge University Press.

Gershunov, A., and D. Cayan. 2008. California heat waves: July 2006 and recent history. *Journal of Climate,* in review.

Graham, N. E. 2005. *Coastal Impacts of North Pacific Winter Wave Climate Variability: The Southern California Bight and the Gulf of the Farallones.* Sacramento, California. Scripps Institution of Oceanography, for the California Energy Commission, PIER Energy Related Environmental Research.

Graham, N. E., and H. F. Diaz. 2001. "Evidence for intensification of North Pacific winter cyclones since 1948." *Bull. Amer. Met. Soc*. 82:1869–1893.

Hansen, J. E. 2005. "A slippery slope: How much global warming constitutes 'dangerous anthropogenic interferenced'? An editorial essay." *Clim. Change.* 68: 269–279, doi:10.1007/s10584-005-4135-0.

Hayhoe K., D. Cayan, C. B. Field, P. C. Frumhoff, E. P. Maurer, N. L. Miller, S. C. Moser, S. H. Schneider, K. N. Cahill, E. E. Cleland, L. Dale, R. Drapek, R. M. Hanemann, L. S. Kalkstein, J. Lenihan, C. K. Lunch, R. P. Neilson, S. C. Sheridan, and J. H. Verville. 2004. "Emissions pathways, climate change, and impacts on California." *PNAS* 101(34): 12422–12427. Aug. 24; Epub Aug. 16, 2004.

Hidalgo, H. G., M. D. Dettinger, and D. R. Cayan. 2008. *Downscaling with Constructed Analogues: Daily Precipitation and Temperature Fields over the United States.* California Energy Commission, PIER Project Report CEC-500-2007-123. 48pp.

Intergovernmental Panel on Climate Change (IPCC) Fourth Assessment Working Group I Report. *Climate Change 2007 The Physical Science Basis.* ISBN 978 0521 88009-1. www.ipcc.ch/ipccreports/ar4-wg1.htm.

Liu, W. T., K. B. Katsaros, and J. A. Businger. 1979. "Bulk Parameterizations of Air-Sea Exchanges of Heat and Water Vapor Including Molecular Constraints at the Interface." *Journal of Atmospheric Science* 36:1722–1735.

Maurer, E. P., I. T. Stewart, C. Bonfils, P. B. Duffy, and D. Cayan. 2007. "Detection, attribution, and sensitivity of trends toward earlier streamflow in the Sierra Nevada." *J. Geophys.* Res. 112, D11118, doi:10.1029/2006JD008088.

Maurer, E. P., and H. G. Hidalgo. 2008. "Utility of daily vs. monthly large-scale climate data: An intercomparison of two statistical downscaling methods." *Hydrology and Earth System Sciences* 12:551–563.

Meehl, G. A., W. M. Washington, W. D. Collins, J. M. Arblaster, A. Hu, L. E. Buja, W. G. Strand, and H. Teng. 2005. "How much more global warming and sea level rise?" *Science* 307(5716): 1769–72.

Miller, N. L., K. Hayhoe, J. Jin, and M. Auffhammer. 2008. "Climate, Extreme Heat, and Electricity Demand in California." *Journal of Applied Meteorology and Climatology* 47:1834–1844.

Neiman, P. J., F. M. Ralph, G. A. Wick, J. D. Lundquist, and M. D. Dettinger. 2008. "Meteorological characteristics and overland precipitation impacts of atmospheric rivers affecting the West Coast of North America based on eight years of SSM/I satellite observations." *J. Hydrometeorology* 9:22–47, doi:10.1175/2007JHM855.1.

O'Reilly, W. C., and R. T. Guza. 1991. "A comparison of spectral refraction and refraction-diffraction wave propagation models." *J. Waterway, Port, Coastal and Ocean Eng.* 117: (3) 199–215.

Pierce, D. W., T. P. Barnett, H. G. Hidalgo, T. Das, C. Bonfils, B. Sander, G. Bala, M. Dettinger, D. Cayan, and A. Mirin. 2008. "Attribution of declining western US snowpack to human effects." J. Climate. In press.

Rahmstorf, S. 2007. "A Semi-Empirical Approach to Projecting Future Sea-Level Rise." Science 315(5810): 368–370, DOI: 10.1126/science.1135456.

Redmond, K. T., and R. W. Koch. 1991. "Surface climate and streamflow variability in the western United States and their relationship to large-scale circulation indices." *Water Resources Research* 27(9): 2381–2399.

Science Daily. 2008. "Global Carbon Emissions Speed Up, Beyond IPCC projections." September 28, 2008. www.sciencedaily.com/releases/2008/09/080925072440.htm.

Stockdon, H. F., R. A. Holman, P. A. Howd, A. H. Sallenger, Jr. 2006. "Empirical parameterization of setup, swash, and runup." *Coast. Eng.* 53: 573–588.

Tolman, H. L. 1999. User manual and system documentation of WAVEWATCH-III version 1.18. NOAA / NWS / NCEP / OMB. Technical note 166, 110 pp.

Trenberth, K. E., and J. W. Hurrell. 1995. *Decadal climate variations in the Pacific.* National Research Council, Natural Climate Variability on Decade-to-Century Time Scales. D. G. Martinson, K. Bryan, M. Ghil, M. M. Hall, T. R. Karl, E. S. Sarachik, S. Sorooshian, and L. D. Talley, Eds. Washington, D.C.: National Academy Press. 472–481.

Wilson, T., et al. 2003. *Global Climate Change and California: Potential Implications for Ecosystems, Health, and the Economy.* California Energy Commission, Sacramento. 1–138.

Wood, A. W., L. R. Leung, V. Sridhar, and D. P. Lettenmaier. 2004. "Hydrologic implications of dynamical and statistical approaches to downscaling climate model outputs." *Climatic Change* 62:189–216.

13.0 Glossary

BCSD	bias correction and spatial downscaling
CA	constructed analogues
CaSLP	California sea level pressure index
CCSM	Community Climate System Model
CNRM	Centre National de Recherches Météorologiques
DJF	December, January, February
ENSO	El Niño/Southern Oscillation
GCM	global climate models
GFDL	Geophysical Fluids Dynamics Laboratory
GHG	greenhouse gas
GtC	gigatonnes of carbon
hPa	hectopascal
Hs	significant wave height
IPCC	Intergovernmental Panel on Climate Change
MAM	March, April, May
MSL	mean sea level
NDJFM	November–March
NCAR	National Center for Atmospheric Research

NCEP	National Centers for Environmental Prediction
NOAA	National Oceanic and Atmospheric Administration
PCM	Parallel Climate Model
ppmv	parts per million, volume
SLP	sea level pressure
SON	September, October, November
SRES	Special Report on Emissions Scenarios
SST	sea surface temperature
SWE	snow water equivalent
SWL	still water level
Tmax	maximum temperature
VIC	Variable Infiltration Capacity hydrological model